

Published in final edited form as:

*Nature*. 2019 October ; 574(7777): 278–282. doi:10.1038/s41586-019-1609-1.

## Structure of the inner kinetochore CCAN complex assembled onto a centromeric nucleosome

Kaige Yan<sup>#1</sup>, Jing Yang<sup>#1</sup>, Ziguo Zhang<sup>#1</sup>, Stephen H. McLaughlin<sup>1</sup>, Leifu Chang<sup>1,4</sup>, Domenico Fasci<sup>2</sup>, Ann E. Ehrenhofer-Murray<sup>3</sup>, Albert J.R. Heck<sup>2</sup>, David Barford<sup>1</sup>

<sup>1</sup>MRC Laboratory of Molecular Biology, Francis Crick Avenue, Cambridge, CB2 0QH, UK

<sup>2</sup>Biomolecular Mass Spectrometry and Proteomics, Bijvoet Center for Biomolecular Research and Utrecht Institute for Pharmaceutical Sciences, University of Utrecht, Padualaan 8, 3584 CH Utrecht, The Netherlands

<sup>3</sup>Humboldt-Universität zu Berlin, Institut für Biologie, Philippstr. 13 Rhoda-Erdmann-Haus, 10099 Berlin, Germany

# These authors contributed equally to this work.

### Abstract

In eukaryotes, accurate chromosome segregation in mitosis and meiosis maintains genome stability and prevents aneuploidy. Kinetochores are large protein complexes, that by assembling onto specialized Cenp-A nucleosomes<sup>1,2</sup>, function to connect centromeric chromatin to microtubules of the mitotic spindle<sup>3,4</sup>. Whereas the centromeres of vertebrate chromosomes comprise Mb of DNA and attach to multiple microtubules, the simple point centromeres of budding yeast are connected to individual microtubules<sup>5,6</sup>. All 16 budding yeast chromosomes assemble complete kinetochores using a single Cenp-A nucleosome (Cenp-A<sup>Nuc</sup>), each of which is perfectly centred on its cognate centromere<sup>7–9</sup>. The inner and outer kinetochore modules are responsible for interacting with centromeric chromatin and microtubules, respectively. Here, we describe the cryo-EM structure of the *S. cerevisiae* inner kinetochore module - the constitutive centromere associated network (CCAN) complex, assembled onto a Cenp-A nucleosome (CCAN–Cenp-A<sup>Nuc</sup>). The structure explains the inter-dependency of CCAN's constituent sub-complexes and shows how the 'Y'-shaped opening of CCAN accommodates Cenp-A<sup>Nuc</sup> to allow specific

Users may view, print, copy, and download text and data-mine the content in such documents, for the purposes of academic research, subject always to the full Conditions of use:[http://www.nature.com/authors/editorial\\_policies/license.html#terms](http://www.nature.com/authors/editorial_policies/license.html#terms)

Correspondence and request for material should be addressed to D.B. (dbarford@mrc-lmb.cam.ac.uk).

<sup>4</sup>Present address: Department of Biological Sciences, Purdue University, IN 47907, USA.

**Data availability and accession codes.** EM maps are deposited with EMDB with accession codes EMD-4580 (CCAN), EMD-4579 (CCAN–Cenp-A<sup>Nuc</sup>), EMD-4581 (Mask1) and EMD-4971 (Mask2). Protein coordinates are deposited with RCSB with accession codes 6QLE (CCAN), 6QLD (CCAN–Cenp-A<sup>Nuc</sup>) and 6QLF (Mask1). The cross-linking mass spectrometry raw files, the associated output and databases are deposited through the ProteomeXchange Consortium via the PRIDE partner repository with the dataset identifier PXD013769. Other data are available upon reasonable request.

**Author contributions.** Z.Z. cloned kinetochore and nucleosome constructs. J.Y. and Z.Z. purified proteins, performed the protein complex reconstitutions and biochemical and genetic analysis. K.Y. and L.C. prepared EM grids, collected and analysed electron microscopy data and determined the three dimensional reconstructions of CCAN–Cenp-A<sup>Nuc</sup> and free Cenp-HIK, respectively. D.B. and K.Y. fitted coordinates, built models, J.Y. and S.H.M. performed SEC-MALS and AUC. D.F. collected and analysed cross-linking mass spectrometry data. A.J.R.H. directed cross-linking mass spectrometry experiments and analysis. A.E.-M. generated the *chl4 cse4-R37A* and *chl4* yeast strains. D.B. directed the project. K.Y. and D.B. wrote the manuscript with help from all authors.

**Author information.** We declare that none of the authors have competing financial or non-financial interests.

CCAN subunits to contact the nucleosomal DNA and histone subunits. Interactions with the unwrapped DNA duplex at the two termini of Cenp-A<sup>Nuc</sup> are mediated predominantly by a DNA-binding groove present in the Cenp-LN sub-complex. Disruption of these interactions impairs assembly of CCAN onto Cenp-A<sup>Nuc</sup>. Our data indicate a mechanism of Cenp-A nucleosome recognition by CCAN and how CCAN acts as a platform for assembly of the outer kinetochore for linking centromeres to the mitotic spindle for chromosome segregation.

The 14 subunit-CCAN complex assembled onto specialized Cenp-A nucleosomes (Cenp-A substituted for histone H3) reconstituted using either an *S. cerevisiae* centromere sequence or the Widom 601 sequence, with both complexes eluting at similar volumes on size exclusion chromatography (Extended Data Fig. 1a-e). In contrast, CCAN did not assemble onto a canonical H3 nucleosome, indicating the specificity of the CCAN – Cenp-A<sup>Nuc</sup> interaction (Extended Data Fig. 1b, f). Cryo-electron micrographs of CCAN–Cenp-A<sup>Nuc</sup> (using the more stable 601-Cenp-A nucleosome) revealed a heterogeneous population of particles that by 3D classification were identified as monomeric free CCAN, a monomer of CCAN in complex with Cenp-A<sup>Nuc</sup>, and dimeric CCAN (Extended Data Figs 2 and 3). A 3D reconstruction of free monomeric CCAN was determined to 3.5 Å resolution (Fig. 1, Extended Data Figs 2 and 3 and Extended Data Table 1). Clearly defined EM density for the majority of amino acid side chains (Extended Data Fig. 4 and Extended Tables 1 and 2) allowed building and refinement of the complete atomic model of CCAN, guided by existing models of individual CCAN subunits. The CCAN–Cenp-A<sup>Nuc</sup> complex at 4.15 Å was built by docking apo CCAN and a nucleosome into the CCAN–Cenp-A<sup>Nuc</sup> EM reconstruction (Fig. 2 and Extended Data Table 1). A cryo-EM reconstruction of uncross linked CCAN–Cenp-A<sup>Nuc</sup>, at lower resolution (Extended Data Fig. 5a), matched that of the cross-linked structure, whereas the free CCAN dimer, determined at 8.6 Å (Extended Data Fig. 5b), resembles the 4.25 Å structure of *S. cerevisiae* CCAN<sup>10</sup>. Compared with the latter study, the Nkp1 and Nkp2 subunit assignments differ.

The arrangement of the three sub-complexes of CCAN; Cenp-LN, Cenp-OPQU+ and Cenp-HIK–TW (Extended Data Table 2), generates a ‘Y’-shaped structure (Fig. 1a, b). The Cenp-N subunit, located at the centre of the ‘Y’, is the coordinating element of CCAN, consistent with it forming a critical node at the centromere–kinetochore interface<sup>11</sup>. Cenp-OPQU+, which has an elongated shape and generates the stem and one arm of the ‘Y’, interacts mainly with Cenp-N. Cenp-L also forms an extensive interface with Cenp-N, and contributes the major point of contact with Cenp-HIK–TW. Together, Cenp-L and Cenp-HIK–TW generate the opposite arm of the ‘Y’ (Fig. 1a, b). The six-subunit Cenp-OPQU+ module shares four subunits in common with vertebrate Cenp-OPQUR, and its structure in CCAN resembles the negative stain reconstruction of human OPQUR<sup>12</sup>. The long N-terminal regions of Cenp-O and Cenp-P, disordered in the *K. lactis* crystal structure<sup>13</sup>, become more structured through interactions with Cenp-HIK and Cenp-N (Fig. 1b, c). Four subunits of Cenp-OPQU+ (Cenp-Q, Cenp-U, Nkp1 and Nkp2) form extended  $\alpha$ -helices that associate in a parallel, inter-weaved fashion to create an irregular coiled-coil  $\alpha$ -helical bundle. This shares a striking similarity to the outer kinetochore complex Mis12<sup>14,15</sup> (Extended Data Fig. 5c). Nkp1 and Nkp2 create an outer layer of  $\alpha$ -helices in Cenp-OPQU+, which are likely substituted by Cenp-R in vertebrates<sup>12</sup>.

The Cenp-HIK module (Fig. 1c), which resembles the free Cenp-HIK complex (Extended Data Fig. 5d), is dominated by the C-terminal HEAT repeats of Cenp-I (Extended Data Fig. 4e). The coiled-coil  $\alpha$ -helices of Cenp-H and Cenp-K run anti-parallel to Cenp-I (Fig. 1c and Extended Data Fig. 4a-c). The base of Cenp-HIK is a four  $\alpha$ -helical bundle comprising the N-termini of Cenp-H and Cenp-K. The flexible head domain, visible in free Cenp-HIK (Cenp-HIK<sup>Head</sup>), and a small population of CCAN particles (Extended Data Figs 3c and 5b, d), matches the shape of the crystal structure of the N-terminal Cenp-I HEAT repeats that are associated with the C-termini of both Cenp-H and Cenp-K<sup>16</sup> (Fig. 1d). The Cenp-TW sub-complex, comprising the histone-fold domain (HFD) subunits Cenp-T and Cenp-W, was not clearly resolved in cryo-EM maps of CCAN and CCAN-Cenp-A<sup>Nuc</sup>. Cenp-TW associates with Cenp-HIK in solution, in agreement with previous studies<sup>11,17</sup>, and Cenp-T<sup>HFDW</sup> interacts equally well with a complex comprising Cenp-HIK<sup>Head</sup> (Extended Data Fig. 1g-j), indicating that the HFDs of Cenp-TW directly interact with Cenp-HIK<sup>Head</sup>.

The relative organization of CCAN subunits in our cryo-EM reconstruction is in agreement with that defined from the *de novo* assembly of the *S. cerevisiae* kinetochore<sup>9</sup> (Extended Data Fig. 1k), and consistent with a negative stain EM reconstruction of the human HIKM-LN-OPQUR complex<sup>12</sup>. To assess the validity of our structure, we performed cross-linking mass spectrometry (XL-MS) analysis of the complexes. Numerous intra and inter-subunit cross-links were identified (Extended Data Fig. 6a, b and Supplementary Tables 1 and 2). Mapping these cross-links onto CCAN and CCAN-Cenp-A<sup>Nuc</sup>, for which both lysines of the cross-linked pair are defined, showed that 95% of the detected crosslinks are within the expected linker distance constraints (Extended Data Fig. 6c-f).

Kinetochores assemble onto Cenp-A<sup>Nuc</sup><sup>9,18</sup>, the hallmark of centromeric chromatin, with the CCAN subunits Cenp-C and Cenp-N directing this assembly<sup>19,20</sup>. In the CCAN-Cenp-A<sup>Nuc</sup> complex, Cenp-A<sup>Nuc</sup> is an octameric nucleosome, with DNA wrapped as a left-handed super-helix (Fig. 2 and Supplementary Video 1), shown previously for free Cenp-A<sup>Nuc</sup><sup>8,21-23</sup>. Also consistent with these reports is that compared with canonical H3 nucleosomes, in the CCAN-Cenp-A<sup>Nuc</sup> complex, the DNA gyre of Cenp-A<sup>Nuc</sup> is more loosely wrapped. In CCAN-Cenp-A<sup>Nuc</sup>, only 105 bp of DNA encircle the Cenp-A-octamer, contrasting with 147 bp for canonical nucleosomes<sup>24</sup> (Figs 2 and 3a-c). A total of 20 bp of DNA are unwrapped equally at each DNA terminus of Cenp-A<sup>Nuc</sup>. One of the unwrapped DNA termini, well defined in cryo-EM density, interacts with CCAN, whereas the other is disordered (Fig. 2a). We observe clearly defined  $\alpha$ -helical density for the N-terminal segment of one Cenp-A subunit (Cenp-A<sup>N</sup>), inserted between the unwrapped DNA duplex and DNA gyre (Figs 2a and 3d).

In the CCAN-Cenp-A<sup>Nuc</sup> complex (Fig. 2 and Supplementary Video 1), Cenp-A<sup>Nuc</sup> inserts end-on into the 'Y'-shaped opening of CCAN with each arm of CCAN embracing opposite sides of the nucleosome. This positions the Cenp-LN module to form extensive contacts with the unwrapped DNA duplex at one of the termini of the Cenp-A<sup>Nuc</sup> DNA gyre (Fig. 2). Cenp-LN adopts a 'U'-shaped structure creating an evolutionarily conserved positively charged groove that engages the unwrapped DNA (Fig. 3c and Extended Data Fig. 7a-c). The DNA duplex runs along the Cenp-LN groove, exiting opposite to the nucleosome (Figs 2 and 3a-c). Cenp-HIK<sup>Head</sup> also functions in Cenp-A<sup>Nuc</sup> recognition because in the CCAN-

Cenp-A<sup>Nuc</sup> complex, EM density corresponding to Cenp-HIK<sup>Head</sup>–Cenp-TW contacts the DNA gyre of Cenp-A<sup>Nuc</sup>, with Cenp-I in close proximity to Cenp-A (Fig. 2d, Extended Data Fig. 3c and Supplementary Video 1). Compared with apo-CCAN, Cenp-HIK<sup>Head</sup>–Cenp-TW rotates ~90° to accommodate Cenp-A<sup>Nuc</sup> (Extended Data Fig. 5e). Previous studies suggested that the vertebrate Cenp-TWSX heterotetramer forms a nucleosome-like particle to interact with DNA<sup>25</sup>. However, this is not compatible with Cenp-TW of budding yeast exactly co-localizing with centromeric Cenp-A<sup>Nuc</sup>, in a Cenp-I-dependent manner<sup>17</sup>. The HFDs of Cenp-TW were assigned to EM density associated with Cenp-HIK<sup>Head</sup> contacting the DNA gyre of Cenp-A<sup>Nuc</sup>, visible in a minor 3D class of CCAN–Cenp-A<sup>Nuc</sup> (Fig. 2e and Extended Data Fig. 3c). On the opposite side of CCAN to Cenp-HIK, the N-terminal regions of Cenp-Q and Cenp-U contact the DNA gyre of Cenp-A<sup>Nuc</sup>, and the N-termini of Cenp-A and H4 (Fig. 2c, f). This is consistent with the Cenp-QU dimer binding DNA<sup>26</sup> and recognising the posttranslational status of the N-terminus of Cenp-A<sup>27</sup>, and further validated by our XL-MS data revealing Cenp-Q crosslinks to H2A and H2B (Extended Data Fig. 6b).

Cenp-N engages Cenp-A<sup>Nuc</sup> in the budding yeast CCAN–Cenp-A<sup>Nuc</sup> complex differently from how the isolated vertebrate Cenp-N subunit interacts with Cenp-A<sup>Nuc</sup> through the L1 loop of Cenp-A and the adjacent DNA gyre<sup>28,29</sup>. Because of steric clashes, the interaction of Cenp-N with Cenp-A<sup>Nuc</sup> revealed in these studies is not compatible with the position of Cenp-N in the context of the CCAN complex (Extended Data Fig. 7d). Binding of Cenp-A<sup>Nuc</sup> at this interface of CCAN, as proposed<sup>10</sup>, would require substantial conformational changes of CCAN. The discrepancy between our structure and that of the vertebrate system, may either reflect genuine species differences in CCAN–Cenp-A<sup>Nuc</sup> architectures, or result from the vertebrate Cenp-N–Cenp-A<sup>Nuc</sup> structure representing an intermediate in the CCAN–Cenp-A<sup>Nuc</sup> assembly pathway, in accordance with CCAN–Cenp-A<sup>Nuc</sup> remodelling during the cell cycle<sup>11</sup>.

Cenp-C also determines kinetochores–Cenp-A<sup>Nuc</sup> interactions<sup>20</sup> and we found that Cenp-C is required for stable assembly onto Cenp-A–*Cen3* nucleosomes (data not shown), although not Cenp-A-601 nucleosomes (Fig. 4b). Cenp-C interacts with Cenp-A through its Cenp-C motif (Extended Data Fig. 5f), similar to vertebrates<sup>30</sup>. However, the regions of Cenp-C associated with CCAN were not visible in the cryo-EM map. XL-MS data indicate that Cenp-C participates in multiple interactions with CCAN (Extended Data Figs 6a, b, g and Supplementary Tables 1 and 2).

To test the validity of the CCAN–Cenp-A<sup>Nuc</sup> structure, we mutated 13 Arg and Lys residues in Cenp-N that line the Cenp-LN–DNA binding groove (Fig. 4a) and tested the ability of the mutant CCAN to assemble onto Cenp-A<sup>Nuc</sup>. To avoid complications of Cenp-C interacting with Cenp-A<sup>Nuc</sup>, we used CCAN without Cenp-C (CCAN<sup>Cenp-C</sup>). The Cenp-N mutant did not impair CCAN<sup>Cenp-C</sup> assembly, and similar to CCAN, CCAN<sup>Cenp-C</sup> binds to Cenp-A-601 nucleosomes, but not H3 nucleosomes (Fig. 4b and Extended Data Figs 8a-c and 9a, b). The Cenp-N mutant disrupted CCAN<sup>Cenp-C</sup>–Cenp-A<sup>Nuc</sup> interactions (Fig. 4b and Extended Data Fig. 8d). In contrast, mutating the L1 loop of Cenp-A did not disrupt the binding of CCAN<sup>Cenp-C</sup> to Cenp-A<sup>Nuc</sup> (Extended Data Figs 8e and 9a).

We then assessed the role of the unwrapped DNA termini of Cenp-A<sup>Nuc</sup> in mediating CCAN – Cenp-A<sup>Nuc</sup> interactions. Because the  $\alpha$ N-helix of the H3 histone stabilizes the wrapped DNA termini of canonical H3 nucleosomes<sup>22,24</sup>, to create a more closed, highly wrapped Cenp-A<sup>Nuc</sup>, we substituted the N-terminal 50 residues of H3 for the N-terminal 140 residues of Cenp-A, creating a chimeric H3<sup>N</sup>-Cenp-A (Extended Data Fig. 7e-g). The resultant H3<sup>N</sup>-Cenp-A<sup>Nuc</sup> wrapped a similar length of DNA as H3<sup>Nuc</sup> (~147 bp) (Extended Data Fig. 9c). The affinity of CCAN<sup>Cenp-C</sup> for H3<sup>N</sup>-Cenp-A<sup>Nuc</sup> was severely disrupted, such that CCAN<sup>Cenp-C</sup> was substantially dissociated from H3<sup>N</sup>-Cenp-A<sup>Nuc</sup> (Fig. 4b and Extended Data Fig. 8g). Binding of H3<sup>N</sup>-Cenp-A<sup>Nuc</sup> to CCAN<sup>Cenp-C</sup> was completely disrupted with the Cenp-N mutant (Fig. 4b and Extended Data Figs 8h). The reduced affinity of CCAN for H3<sup>N</sup>-Cenp-A<sup>Nuc</sup> is not due to the lack of the Cenp-A N-terminus because CCAN bound to Cenp-A<sup>Nuc</sup> and <sup>N</sup>Cenp-A<sup>Nuc</sup> equally well (Fig. 4b and Extended Data Fig. 8c, f). These biochemical studies confirm the CCAN – Cenp-A<sup>Nuc</sup> cryo-EM structure showing that CCAN interacts with the unwrapped DNA termini of Cenp-A<sup>Nuc</sup>, and that a major role of the Cenp-LN DNA-binding groove is to engage the unwrapped DNA gyre of Cenp-A<sup>Nuc</sup> (Fig. 3c).

Disruption of the budding yeast Cenp-N gene (*CHL4*) causes chromosome loss and instability, without affecting viability<sup>31</sup>. However, combining a *chl4* deletion with either mutation of Cenp-A (*CSE4*), or deletion of other kinetochore subunits, results in synthetic growth defects and lethality<sup>9,27</sup>. Cenp-N is an essential gene in *S. pombe* and humans. To investigate the *in vivo* consequences of disrupting the DNA-binding groove of Cenp-LN, we tested whether the synthetic growth defect of the *chl4 cse4-R37A* mutant at 37 °C<sup>27</sup> is rescued by Cenp-N<sup>Mut</sup>. Whereas wild type Cenp-N rescued the growth defect of the *chl4 cse4-R37A* mutant, the Cenp-N<sup>Mut</sup> did not (Fig. 4c-e). This result demonstrates a functional role for the Cenp-LN DNA-binding groove, and together with our biochemical data (Fig. 4b and Extended Data Fig. 8), supports the CCAN – Cenp-A<sup>Nuc</sup> architecture we report here. In budding yeast, Cenp-A<sup>Nuc</sup> is linked to the outer kinetochore Ndc80 complex and associated microtubules through a pathway comprising the essential proteins Cenp-C, Cenp-QU and the Mis12 complex, and by a second pathway involving Cenp-TW and Cenp-N<sup>9</sup> (Extended Data Fig. 1k). The location of Cenp-N at the centre of CCAN is consistent with these two pathways. The unwrapped DNA termini of Cenp-A<sup>Nuc</sup> contribute to stabilizing the CCAN – Cenp-A<sup>Nuc</sup> complex through the Cenp-LN DNA binding groove, augmented by contacts of both Cenp-A and the Cenp-A<sup>Nuc</sup> DNA gyre with Cenp-C (Extended Data Fig. 5f), Cenp-LN (Fig. 3c), Cenp-TW, Cenp-HIK<sup>Head</sup> and Cenp-QU<sup>27</sup> (Fig. 2d-f).

In the cryo-EM reconstruction, Cenp-A<sup>Nuc</sup> is associated with a single CCAN, whereas the expected stoichiometry is two CCANs to Cenp-A<sup>Nuc</sup><sup>32</sup>. SEC-MALS and AUC confirmed the reconstituted CCAN–Cenp-A<sup>Nuc</sup> is consistent with two CCANs per Cenp-A<sup>Nuc</sup> (Extended Data Fig. 10a-g). In a generated model of dimeric CCAN–Cenp-A<sup>Nuc</sup>, two CCAN complexes associate through their tips of the ‘Y’, creating a slot that perfectly accommodates Cenp-A<sup>Nuc</sup> that is inserted vertically (Fig. 4f). The two CCAN complexes cradle Cenp-A<sup>Nuc</sup> with its unwrapped DNA duplexes stretched out, over-lying CCAN’s DNA-binding surface, consistent with XL-MS cross-links between Cenp-Q and Cenp-TW (Extended Data Fig. 6b). Extensive 2D classification of the cryo-EM data identified 2D classes of dimeric CCAN–Cenp-A<sup>Nuc</sup> particles with two-fold symmetry axes (Extended

Data Fig. 2c). These particles correspond closely to the calculated reprojections of the proposed dimeric CCAN–Cenp-A<sup>Nuc</sup> complex (Extended Data Fig. 10h). Cryo-EM grids destabilize CCAN – Cenp-A<sup>Nuc</sup>, resulting in a very low abundance of dimeric CCAN–Cenp-A<sup>Nuc</sup> particles.

In *S. cerevisiae*, the CBF3 complex engages the CDEIII element of the ~125 bp centromere to direct Cenp-A/Cse4 nucleosome deposition. Modelling indicates that only when bound to a single CCAN promoter can Cenp-A<sup>Nuc</sup> simultaneously accommodate CBF3 (Extended Data Fig. 9d), suggesting that CBF3 would not associate with a fully assembled kinetochore.

The dimeric CCAN–Cenp-A<sup>Nuc</sup> complex suggests two possibilities for how a kinetochore-attached microtubule would segregate centromeric chromatin (Extended Data Fig. 10i, j and Supplementary Video 2). In one scenario, CCAN attaches to the microtubule through the outer kinetochore, using the same face as its DNA-binding surface (Extended Data Fig. 10i). This would sandwich the DNA between CCAN and the outer kinetochore, a possibility compatible with the long flexible linkers that attach CCAN to the outer kinetochore. As the microtubule pulls on the kinetochore, CCAN would hoist the over-lying DNA. Alternatively, microtubules could attach to CCAN from the opposite face to its DNA-binding surface, so the chromosome is pulled from behind the inner kinetochore (Extended Data Fig. 10j). Because vertebrate Cenp-A<sup>Nuc</sup> also wraps between 100-120 bp (of  $\alpha$ -satellite DNA)<sup>22</sup>, with nucleosome unwrapping enhanced by Cenp-C<sup>33</sup>, and the human CCAN architecture<sup>12</sup> is similar to yeast, it is likely that the mechanism of recognition of the specialized Cenp-A nucleosome, we describe here for the budding yeast inner kinetochore, is evolutionarily conserved.

## Methods

### Cloning, expression, purification and reconstitution of recombinant CCAN–Cenp-A<sup>Nuc</sup> nucleosome complex

**Cloning**—The genes for *CTF19*, *OKP1*, *MCM21*, *AME1*, *NKP1*, *NKP2*, *CTF3*, *MCM16*, *MCM22*, *CNN1*, *WIP1*, *MIF2*, *CHL4* and *IML3* (*MCM19*) (Extended Data Table 2 for vertebrate Cenp conversion) were amplified by PCR from *Saccharomyces cerevisiae* genomic DNA and cloned into a pU1 plasmid using a modified Multibac expression system<sup>34</sup>. The intron in *MCM21* was deleted by USER methodology. A double StrepII tag together with a TEV cleavage site was attached to the C-termini of Ame1, Ctf3, Chl4, Mif2 and Cnn1 proteins. For expression of the Cenp-OPUQ+ complex (COMA+: Ctf19, Okp1, Mcm21, Ame1, Nkp1 and Nkp2) gene expression cassettes in pU1 were subsequently cloned into a pF2 vector<sup>34</sup>. The gene expression cassettes for *CTF3*, *MCM16*, *MCM22*, *CNN1* and *WIP1* were cloned into pF2 to generate the Cenp-HIK–TW complex.

**Cenp-HIK-TW complexes**—To test which regions of Cenp-H, Cenp-I and Cenp-K interact with each other and with Cenp-TW, the following fragments of Cenp-H, Cenp-I and Cenp-K were constructed: Cenp-I (residues 1-308) (Cenp-I<sup>N</sup>), Cenp-H (residues 137-182) (Cenp-H<sup>C</sup>), Cenp-H (residues 130-239) (Cenp-K<sup>C</sup>) and combinations of Cenp-H, Cenp-I and Cenp-K, together with Cenp-TW were for assembled into the pU1 plasmid for Multibac

expression<sup>34</sup> for co-expression using the insect cell/baculovirus system. A double StrepII tag was added to C-terminus of Cenp-I.

To test the role of the positively-charged DNA-binding groove of Cenp-N for Cenp-A nucleosome interactions, a total of 13 Arg and Lys mutations were introduced into *CHL4* (Cenp-N<sup>Mut</sup>) by total gene synthesis (GeneArt/Thermo Fischer): *chl4*<sup>K22/K26S/R67S/K100S/K103S/K105S/R198S/K217S/K245S/K249S/K384S/K401S/K403S</sup>. Cenp-N<sup>Mut</sup> was combined with Cenp-L to generate a Cenp-N<sup>Mut</sup>-Cenp-L co-expression baculovirus.

The baculoviruses for expression of Cenp-OPQU+, Cenp-HIK-TW, Cenp-C and Cenp-LN were prepared for expression using the insect cell-baculovirus system<sup>34</sup>.

The cDNA encoding for *Saccharomyces cerevisiae CSE4* (*S. cerevisiae CENP-A*), *H2A*, *H2B* and *H4* histone genes were synthesized (GeneArts/Thermo Fisher) with optimized codons for expression in *Escherichia coli* and were subsequently cloned into pET28A with a TEV protease cleavable N-terminal His<sub>6</sub> tag. For the recombinant Cse4 octamer (*ScCenp-A* octamer), four expression cassettes for *CSE4*, *H2A*, *H2B* and *H4* histone genes were subsequently cloned into a single pET28 plasmid by USER methodology for *E. coli* expression. For *ScH3* octamer purification *CSE4* was replaced by the *H3* gene. The Cenp-A L1 loop mutant (Cenp-A<sup>L1</sup>: *cse4*<sup>K172S/D173A/Q174A/D175S</sup>) and *cse4*<sup>130-229</sup> (N<sup>Cenp-A</sup>) were expressed for producing Cenp-A<sup>L1</sup> and Cenp-A<sup>N</sup> octamers and nucleosomes, respectively. The chimeric H3<sup>N</sup>-Cenp-A histone comprises a fusion of residues 1-50 of *ScH3* with residues 141-229 of *CSE4*. The H3<sup>N</sup>-Cenp-A histone (molecular mass 15.74 kDa) was used to generate H3<sup>N</sup>-Cenp-A<sup>Nuc</sup>-601 by the same procedure as for Cenp-A<sup>Nuc</sup>.

**Expression and purification**—Complexes of Cenp-OPQU+, Cenp-HIK, Cenp-HIK-TW, Cenp-LN and Cenp-C were expressed individually in High-5 insect cells (*Trichoplusia ni*: expression system). The High-5 insect cell line was not tested for mycoplasma contamination and was not authenticated. The cells were harvested 48 h after infection. The lysate was loaded onto a Strep-Tactin® Column (Qiagen) and the complexes were eluted with 2.5 mM desthiobiotin (Sigma) in a buffer of 50 mM Tris.HCl (pH 8.0), 200 mM NaCl, 1 mM DTT. The StrepII-tag was cleaved using TEV protease overnight at 4°C. The proteins and complexes were further purified on Resource Q anion exchange and size exclusion chromatography in a buffer of 20 mM Hepes (pH 8.0), 200 mM NaCl, 2 mM DTT. Free Cenp-HIK was cross-linked using 0.05% glutaraldehyde for 8 min on ice and quenched with 50 mM Tris.HCl (pH 8.0), then further purified using Superose 6 size exclusion chromatography. The proteins and complexes were collected, concentrated, frozen in liquid nitrogen and stored at -80°C. The stable 14-subunit CCAN complex was reconstituted by combining individually purified CCAN sub-complexes; Cenp-LN, Cenp-OPQU together with the budding yeast-specific Nkp1 and Nkp2 subunits (Cenp-OPQU+), Cenp-HIK-TW and Cenp-C.

For Cenp-HIK-TW assembly assays, a combination of full length and either their N or C terminal fragments of Cenp-I, Cenp-H and Cenp-K were co-expressed together with Cenp-T and Cenp-W or with Cenp-T<sup>HFD</sup> (residues 268-361) and Cenp-W. Affinity purified complexes were analysed using SDS-PAGE analysis.

The *ScCenp-A* octamer was prepared by co-expression of *CSE4*, *H2A*, *H2B* and *H4* in B834<sup>Rare2</sup> *E. coli* cells. The harvested cell pellet was lysed in a buffer of 50 mM Tris.HCl (pH 8.0), 2 M NaCl. The *ScCenp-A* octamer was isolated by Ni-NTA affinity chromatography, eluted with imidazole in 2 M NaCl buffer. The octamer was further purified by S200 size exclusion chromatography, concentrated to 3 mg/mL in a buffer of 10 mM Tris.HCl (pH 7.5), 2 M NaCl, 1 mM EDTA and 2 mM DTT and frozen in liquid nitrogen and stored at -80°C.

For DNA fragment preparation, NEB Stable *E. coli* cells containing a plasmid with a multiple copy (20x) of the 147 base pair Widom 601 sequence flanked by EcoRV sites in a pUC18 backbone (gift from Fabrizio Martino, MRC-LMB) were cultured in LB broth with ampicillin. The plasmid was isolated by using the Plasmid Giga Kit (Qiagen). The Widom 601 fragment was purified with a 1 mL resource Q anion exchange chromatography column (GE Healthcare Life Sciences) after over-night digestion with EcoRV-HF (NEB). The purified DNA was precipitated, dissolved, buffer-exchanged and stored in a buffer of 2 M NaCl, 10 mM Tris.HCl (pH 7.5), 1 mM EDTA, 2 mM DTT at -20°C. *CEN3* DNA fragment was prepared by the primer-extension method. Two oligos used were: CEN3F ATAAGTCACA TGATGATATT TGATTTTATT ATATTTTTTAA AAAAAGTAAA AAATAAAAAG TAGTTTATTT TTAATAAATA AAATTTAAAA and CEN3R TTCAATGAAA TATATATTTT TACTATTTT TTTTAACT TTCGGAAATC AAATACACTA ATATTTTAAA TTTTATTTTT TAAAAATAAA CTA (Sigma-Aldrich). The fragment was produced in a one step extension at 68 °C for 1 min. The final product of the 153 base pair *CEN3* (ATAAGTCACA TGATGATATT TGATTTTATT ATATTTTTTAA AAAAAGTAAA AAATAAAAAG TAGTTTATTT TTAATAAATA AAATTTAAAA TATTAGTGTA TTTGATTTCC GAAAGTTAAA AAAGAAATAG TAAGAAATAT ATATTTTCATT GAA) fragment was purified using a 1 mL resource Q anion exchange chromatography and stored in a buffer of 2 M NaCl, 10 mM Tris.HCl (pH 7.5), 1 mM EDTA, 2 mM DTT at -20°C.

**ScCenp-A nucleosome and derivatives preparation**—*ScCenp-A*, Cenp-A-L1<sup>Mut</sup>, <sup>N</sup>Cenp-A, H3<sup>N</sup>-Cenp-A and H3 histone octamers were wrapped by gradient dialysis from 2 M NaCl to 100 mM NaCl buffer with 10 mM Tris.HCl (pH 7.5), 1 mM EDTA and 2 mM DTT. *ScCenp-A* octamer was mixed with either 601 DNA or *CEN3* DNA, at 7.8 μM concentration. The mixture in the dialysis tube was inserted into a 500 mL beaker containing 500 mL buffer of 2 M NaCl, 10 mM Tris.HCl (pH 7.5), 1 mM EDTA, 2 mM DTT. The NaCl concentration in the dialysis buffer was gradually decreased to 100 mM using an Akta pump at 1.5 mL min<sup>-1</sup> for 16 hours at 4°C. The mixture was further dialysed against the buffer of 100 mM NaCl, 10 mM Tris.HCl (pH 7.5), 1 mM EDTA, 2 mM DTT for 4 hours at 4°C. The *ScCenp-A* nucleosome and derivatives were stored at 4°C.

**Reconstitution of CCAN–Cenp-A nucleosome complex**—The CCAN–Cenp-A nucleosome complex was reconstituted by mixing purified Cenp-C and Cenp-LN with Cenp-A nucleosome followed by Cenp-HIK–TW and Cenp-OPQU+. The stoichiometry of CCAN sub-complexes to Cenp-A<sup>Nuc</sup> was adjusted so that CCAN sub-complexes were in excess, as judged by their separation from CCAN–Cenp-A<sup>Nuc</sup> by size exclusion

chromatography. The mixed sample was dialysed over-night in a buffer of 10 mM Hepes (pH 8.0), 80 mM NaCl, 1 mM EDTA and 0.5 mM TCEP at 4 °C. CCAN–Cenp-A<sup>Nuc</sup> was purified by Superose 6 size exclusion chromatography. For cryo-EM analysis, CCAN–Cenp-A<sup>Nuc</sup> was cross-linked with 5 mM BS3 (Thermo Fisher Scientific) for one hour on ice and quenched with 50 mM Tris and then subjected to further size exclusion chromatography with an Agilent Bio SEC-5 column (Agilent Technologies) before preparing cryo-EM grids. Mild cross-linking of CCAN–Cenp-A<sup>Nuc</sup> reduced dissociation of CCAN from Cenp-A<sup>Nuc</sup> during preparation of cryo-EM grids. To assess whether cross-linked created artefacts, we also collected a cryo-EM data set using uncross-linked CCAN–Cenp-A<sup>Nuc</sup>.

**SEC analysis of CCAN–Cenp-A<sup>Nuc</sup> complexes**—To analyse the formation and stability of CCAN–Cenp-A<sup>Nuc</sup> complexes and mutants in CCAN and Cenp-A, all CCAN–Cenp-A<sup>Nuc</sup> complexes were assembled as above (with or without Cenp-C) and then applied to an Agilent Bio SEC-5 size exclusion chromatography column. The eluted fractions were analysed on SDS PAGE gels and stained with Coomassie Blue and ethidium bromide to detect proteins and DNA. For assembly of the CCAN–Cenp-A<sup>Nuc</sup> complexes, the concentration of Cenp-A<sup>Nuc</sup> was 1.6  $\mu$ M, and that for the individual CCAN sub-complexes (1.6  $\mu$ M).

**Multi-angle light scattering**—SEC-MALS was performed using a Wyatt MALS system. CCAN alone, uncross-linked and BS3 cross-linked CCAN–Cenp-A<sup>Nuc</sup> complexes were injected onto an Agilent Bio SEC-5 column gel filtration column pre-equilibrated in 10 mM Hepes (pH 7.5), 80 mM NaCl, 1 mM EDTA and 0.5 mM TCEP. The light scattering and protein concentration at each point across the peaks in the chromatograph were used to determine the absolute molecular mass from the intercept of the Debye plot using Zimm's model as implemented in the ASTRA v5.3.4.20 software (Wyatt Technologies). To determine inter-detector delay volumes, band-broadening constants and detector intensity normalization constants for the instrument, we used aldolase as a standard prior-to sample measurement. Data were plotted with the program PRISM v8.2.0 (GraphPad Software Inc.).

**Analytical ultracentrifugation**—Uncross-linked and BS3 cross-linked CCAN–Cenp-A<sup>Nuc</sup> complex at approximately 1 mg/mL in 10 mM Hepes (pH 7.5), 80 mM NaCl, 1 mM EDTA and 0.5 mM TCEP were subjected to velocity sedimentation at 40,000 rpm at 4 °C in an An50Ti rotor using an Optima XL-I analytical ultracentrifuge (Beckmann). The data were analysed in SEDFIT 16.1<sup>35</sup> using a c(s) distribution model. The partial-specific volumes ( $v$ -bar) were calculated using Sednterp (v20130813 beta) (Dr Thomas Laue, University of New Hampshire). The density and viscosity of the buffer were determined with a DMA 4500M density meter (Anton Parr) and an AMVn viscometer (Anton Paar). Data were plotted with the program GUSI<sup>36</sup>.

**Micrococcal nuclease digestion assay**—Nucleosomes were digested for 40 min with 1 unit of MNase (NEB) per microgram of DNA at room temperature (22 °C). Reactions were terminated with the addition of excess EGTA. The digested nucleosome mixtures were loaded onto an agarose gel and stained to visualize the DNA.

**Yeast strains and growth analysis**—The *S. cerevisiae* strain with a *chl4* deletion and *cse4-R37A* mutation (*chl4 cse4-R37A*), AEY4992 (*MAT $\alpha$  ade2-101 lys2 his3-11,15 trp1-1 leu2-3,112 ura3-1 can1-100 chl4 ::kanMX cse4-R37A*) and wild type *S. cerevisiae* strain (W303) (*MAT $\alpha$  ade2-101 his3-11,15 trp1-1 leu2-3,112 ura3-1*) were described and authenticated in <sup>27,37</sup>. Yeast strains do not have mycoplasma and were not tested for mycoplasma contamination. Cenp-N<sup>WT</sup> and Cenp-N<sup>Mut</sup> strains were created by transforming AEY4992 <sup>27,37</sup> with a 2 $\mu$  origin plasmid pYes2 incorporating either *CHL4*<sup>WT</sup> or *chl4*<sup>Mut</sup> (*chl4*<sup>K22/K26S/R67S/K100S/K103S/K105S/R198S/K217S/K245S/K249S/K384S/K401S/K403S</sup>) with *CHL4*'s native promoter, a C-terminal double StrepII-tag on Chl4, and the *URA3* selection marker. The transformed cells were selected on synthetic media lacking uracil, and the presence of the plasmid-encoded *CHL4* was verified by PCR using a primer pair over-spanning the *CHL4* and *URA3* genes. Cells were grown in drop-out uracil (SC-U) medium at 30°C and spotted in tenfold dilution steps on YPED plates. The plates were incubated at either 30°C or 37°C for three days.

**Immunoprecipitation and Western blotting for detecting Cenp-N expression in the *chl4 cse4-R37A* yeast**—Six litres of synthetic SC-U culture were inoculated with the *chl4 cse4-R37A* yeast strain transformed with the pYes2 plasmid expressing either wild type or mutant Cenp-N with a C-terminal double StrepII-tag (and empty vector control) and harvested at OD<sub>600</sub> of ~0.8. Pelleted cells were lysed in buffer (50 mM Tris, pH 8.0, 300 mM NaCl, 1 mM EDTA, 1 mM DTT) and the cleared lysate was loaded onto a 1 mL Strepactin column. Fractions were eluted with 5 mM desthiobiotin and analysed by SDS PAGE. Western blotting was performed with an anti-Strep antibody (MCA2489P, Bio-Rad) that detected the C-terminal double StrepII-tag on Cenp-N. Total protein was analysed by Coomassie blue staining for loading controls (normalized loading).

**Electron microscopy data collection**—3.0  $\mu$ l of the CCAN–Cenp-A<sup>Nuc</sup> complex at a concentration of ~1 mg/mL was applied to glow-discharged copper 300 mesh Quantifoil R1.2/1.3 holey carbon grids (Quantifoil Micro Tools GmbH) (no carbon support). The grids were flash frozen by being plunged into liquid ethane using an FEI Vitrobot Mark IV (waiting time, 20 s, blotting time, 2 s). EM image stacks were collected with Falcon III cameras in counting mode on four different FEI Titan Krios electron microscopes at a nominal magnification of 75 K (yielding pixel sizes of 1.065 Å, 1.070 Å, 1.085 Å, 1.090 Å, respectively). The images were recorded at a dose rate of 0.6 electrons per pixel per second and the total exposure time was 60 s (75 frames) with the FEI automated low-dose data-collection program EPU. Defocus varied from -2.0 to -2.8  $\mu$ m with an interval of 0.2  $\mu$ m.

For the isolated Cenp-HIK sample, freshly purified Cenp-HIK complex was first visualized by negative-staining EM to check the sample quality. Aliquots of 3  $\mu$ l samples at ~0.2 mg/mL were applied onto glow-discharged Quantifoil R1.2/1.3 300-mesh holey carbon grids. The grids were incubated for 30 s at 4 °C and 100% humidity and then blotted for 8 s and plunged into liquid ethane using an FEI Vitrobot III. Grids made in this way showed strong preferred orientation. To overcome this problem, we treated the Cenp-HIK complex with 0.025% glutaraldehyde for 10 min on ice before size exclusion chromatography

purification. More views were observed after this treatment, allowing us to reconstruct the 3D structure.

For the isolated Cenp-HIK sub-complex, images were collected using EPU with a Falcon III detector in counting mode. 910 micrographs were collected using a dose rate of 0.5 electrons per pixel per second and a total exposure time of 60 s. Each micrograph was recorded into a movie stack of 75 frames. Calibrated physical pixel size is 1.38 Å/pixel.

**Image processing**—Movie frames were first aligned using MotionCor2<sup>38</sup>. CTF parameters were estimated with Gctf<sup>39</sup>. The initial template-free particle picking was performed with Gautomatch (developed by Kai Zhang, <http://www.mrc-lmb.cam.ac.uk/kzhang/Gautomatch/>). Subsequent image processing was carried out using RELION 2.1 and RELION 3.0<sup>40,41</sup>. A subset of 556 micrographs (of 1582) was used for Gautomatch template-free particle picking, and the resulting 119,143 coordinates were imported into RELION 2.1 for particle extraction and reference-free 2D classification. Selected averages from the 2D classification were used for an initial model reconstruction with SIMPLE-PRIME<sup>42</sup>. These 2D class averages were used for template-based particle auto-picking in Gautomatch for the entire dataset. The extracted particles were subject to two rounds of reference-free 2D classifications resulting in a dataset of 1,385,496 particles from the combined total of 9,002 micrographs. A tandem cascade of 3D classifications against the model built with SIMPLE-PRIME<sup>42</sup> was performed, and initial iterations were performed without angular search restriction for each round of classification. After removing the bad particles, 424,577 particles were assigned to CCAN, whereas 193,882 were assigned to the CCAN–Cenp-A<sup>Nuc</sup>, which were used for the subsequent Bayesian polishing, multi-body refinement, and the final map refinement and atomic coordinate refinement. Beam-tilt parameters of the particles were estimated based on the individual dataset, and they were applied during the Bayesian polishing of each dataset in RELION 3.0. 3D refinements and multi-body refinements were performed with the polished particle stacks after merging all the datasets. The dataset including all the particles generated the highest resolution reconstruction with an overall CCAN mask. The final resolutions for CCAN and CCAN–Cenp-A<sup>Nuc</sup> are 3.55 Å and 4.15 Å, respectively, based on the gold-standard FSC=0.143 criterion<sup>43</sup> (Extended Data Fig. 2d).

To identify dimeric CCAN–Cenp-A<sup>Nuc</sup> particles, five 2D classes, whose 2D averages of CCAN–Cenp-A<sup>Nuc</sup> (Extended Data Fig. 2c) showed smeared density in close proximity to Cenp-A<sup>Nuc</sup>, were selected for further analyses. The selected particles (10, 553 particles) were subject to a tandem cassette of 2D classifications, resulting in 556 particles, which showed clear C2-symmetry 2D averages. These particles were re-extracted from the micrographs with a box size of 400 pixels to accommodate the bigger symmetric particles. The re-extracted particles were then subject to further 2D classification, and classified into 20 classes, generating the representative symmetric 2D averages shown in the red box of Extended Data Fig. 2c. The reprojections of the modelled dimeric-CCAN–Cenp-A<sup>Nuc</sup> map (filtered to 20 Å resolution) were generated with `relion_project`. The projections are shown as Extended Data Fig. 10h. The small number of particles and highly preferred orientation on the EM grid (in the plane of the 2-fold symmetry axis) precluded a 3D reconstruction.

**Multi-body refinement**—To improve map resolution we performed multi-body refinement (MBR) in RELION 3.0<sup>41</sup>. Two masks were generated. Mask1 comprised Cenp-LN-OPQU+, excluding Cenp-HIK. Mask2 comprised Cenp-HIK and portions of Cenp-N, L, O and P, (Extended Data Figs 2h, i and 3b). The resultant maps were determined at 3.45 Å and 3.83 Å resolution, respectively. To further improve regions at the periphery of Cenp-OPQU+, partial signal subtracted particles (Cenp-HIK subtracted) were used for a second round of multi-body refinement. Mask3 included part of Cenp-N and N-terminal regions of Cenp-Q, Cenp-U, Nkp1 and Nkp2 with small regions of Cenp-O and Cenp-P. Mask4 comprised Cenp-OP, Cenp-LN and C-terminal regions of Cenp-QU, Nkp1 and Nkp2. Multi-body refinement based on mask3 and mask4 resulted in 3.92 Å and 3.49 Å maps, respectively. The resultant maps derived using multi-body refinement based on the four masks showed significantly improved definition of EM densities and were used for model building (Extended Data Figs 2d, h, i and 3b). Careful choice of the boundaries of mask2 was critical to optimizing the EM density quality for Cenp-HIK. Including specific regions of Cenp-N, L, O and P within mask2 was critical to generating maps that allowed side chain definition of the coiled-coil regions of Cenp-H and Cenp-K (Extended Data Fig. 4a). This defined the correct assignment and polarity of these chains. MBR also improved definition of side chains in the base of Cenp-HIK. The subsequent multi-body refinement using mask3 and mask4 improved side chain definition for the peripheral regions of Cenp-OPQU+. Portions of the EM density map are shown in Extended Data Fig. 4. A 3D class (4% of total apo-CCAN) corresponding to dimeric apo-CCAN was determined at 10 Å resolution (Extended Data Fig. 3a).

For the uncross-linked dataset, the same procedures were applied. 123,215 particles from 1,586 micrographs were used for the final reconstruction of a map at 7.8 Å resolution for the CCAN–Cenp-A<sup>Nuc</sup> complex (Extended Data Fig. 5a).

For the isolated Cenp-HIK complex, the same procedure was applied. 374,158 particles were used for the final reconstruction of a map at 4.3 Å resolution for Cenp-HIK complex.

Before visualization, a negative B factor determined with RELION 2.1 was applied to the density map for sharpening. The modulation transfer function (MTF) of the detector was corrected in the post-processing step with RELION 3.0<sup>40</sup>. The local resolution was estimated with RELION 3.0<sup>40</sup>.

### Model building and structure refinement

**Apo-CCAN**—EM density maps were visualized in COOT<sup>44</sup> and Chimera<sup>45</sup>. The crystal structure of *K. lactis* Cenp-OPQ (PDB:5MU3)<sup>46</sup> (equivalent to *S. cerevisiae* Cenp-O residues 159 to 362, *S. cerevisiae* Cenp-P residues 148 to 361 and *S. cerevisiae* Cenp-Q residues 320 to 342) and structures of *S. cerevisiae* Cenp-N (residues 374 to 450), Cenp-L (PDB:4JE3)<sup>47</sup> and human Cenp-N N-terminal domain (NTD) (PDB: 6EQT)<sup>29</sup> (equivalent to residues 12 to 260 of *S. cerevisiae* Cenp-N) were fitted into the cryo-EM density maps of apo-CCAN, with refitting and mutating to the *S. cerevisiae* sequence for Cenp-N<sup>NTD</sup>, Cenp-O, Cenp-P and Cenp-Q. Based on the excellent quality of the EM densities, atomic models of Nkp1, Nkp2, Cenp-U, Cenp-Q, Cenp-H (residues 7 to 136), Cenp-I (residues 321 to 728) and Cenp-K (residues 4 to 128) and the inter-domain region of Cenp-N (residues 261 to 373)

were built *de novo*. Only short stretches of Cenp-Q (residues 161 to 216) and Cenp-U (residues 131 to 155) were built as polyAla (Extended Data Table 2). The secondary-structural and disordered regions of the protein sequences were analysed with PHYRE2<sup>48</sup> and PSIPred<sup>49</sup>. A model for the Cenp-HIK head domain was based on the crystal structure of regions of the Cenp-HIK assembly from *C. thermophilum* and *T. terrestris* (PDB 5Z08)<sup>16</sup> corresponding to *S. cerevisiae* Cenp-H (residues Asp143 to Ile181), Cenp-I (residues Leu5 to Ala241) and Cenp-K (residues Ala136 to Thr236) and derived using PHYRE2<sup>48</sup>. The 3.5 Å monomeric free CCAN coordinates were rigid-body docked into the cryo-EM map. The Cenp-HIK head domain was fitted to EM density of the dimeric apo-CCAN. A linker region that connects Cenp-N<sup>NTD</sup> with Cenp-N<sup>CTD</sup>, not present in crystal structures, was built *de novo*.

**CCAN–Cenp-A<sup>Nuc</sup>**—The CCAN complex model was then fit into the CCAN–Cenp-A<sup>Nuc</sup> cryo EM map. The nucleosome was modelled on the *S. cerevisiae* H3 nucleosome (PDB: 1ID3)<sup>50</sup> with *S. cerevisiae* Cenp-A modelled on *H. sapiens* Cenp-A (PDB: 3AN2)<sup>22</sup> and mutated to the *S. cerevisiae* Cenp-A sequence, and the 601 Widom DNA sequence (PDB: 3LZ0)<sup>51</sup>. The Cenp-C model (PDB: 4X23)<sup>30</sup> in the centromeric nucleosome was rigid body-docked into the EM density.

The apo-CCAN and CCAN–Cenp-A<sup>Nuc</sup> models (excluding the Cenp-HIK head domains) were optimized by several rounds of real-space refinement using PHENIX (phenix.real\_space\_refine)<sup>52</sup>. Standard stereochemical and secondary structural constraints were applied during the real-space refinement. The final models were evaluated with COOT<sup>44</sup>, PHENIX<sup>52</sup> and MolProbity (<http://molprobity.biochem.duke.edu/>)<sup>53</sup>. Figures were prepared using ChimeraX<sup>54</sup>, Chimera<sup>45</sup>, and PyMOL (Molecular Graphics System, 2.0.3, Schrodinger, LLC). Details of the fitted and refined coordinates in Extended Data Table 2. Multiple sequence alignments were performed and displayed using JALVIEW<sup>55</sup>.

**Cross-linking mass spectrometry analysis**—To assess the validity of our structure, we performed cross-linking mass spectrometry (XL-MS) analysis of the complexes<sup>56</sup>. Three independent crosslinking reactions were performed for each sample. The CCAN or CCAN–Cenp-A<sup>Nuc</sup> complexes in 20 mM HEPES pH 7.5, 80 mM NaCl and at a concentration of 3 mg/mL were crosslinked with 1 mM DSSO for 15 min at room temperature. Each reaction was quenched with Tris.HCl (pH 8.0) to 50 mM and supplemented with urea to 8 M. The samples were reduced by addition of DTT at a final concentration of 10 mM for 1 hour at room temperature, and alkylated for 0.5 hour at room temperature in the dark by addition of iodoacetamide to 50 mM. Protein digestion was performed with Lys-C at an enzyme-to-protein ratio of 1:75 (w/w) at 30 °C for 3 hours, then the samples were diluted in 50 mM ammonium bicarbonate and further digested with trypsin at an enzyme-to-protein ratio of 1:75 (w/w) at 37 °C for 16 hours. The digested samples were acidified with formic acid to 1%, desalted using home-made C18 stage tips, dried and stored at –80 °C for further use.

Each sample was analysed by LC-MS/MS using an Agilent 1290 Infinity System (Agilent Technologies) in combination with an Orbitrap Fusion Lumos (Thermo Scientific). Reverse phase chromatography was carried out using a 100-µm inner diameter 2-cm trap column

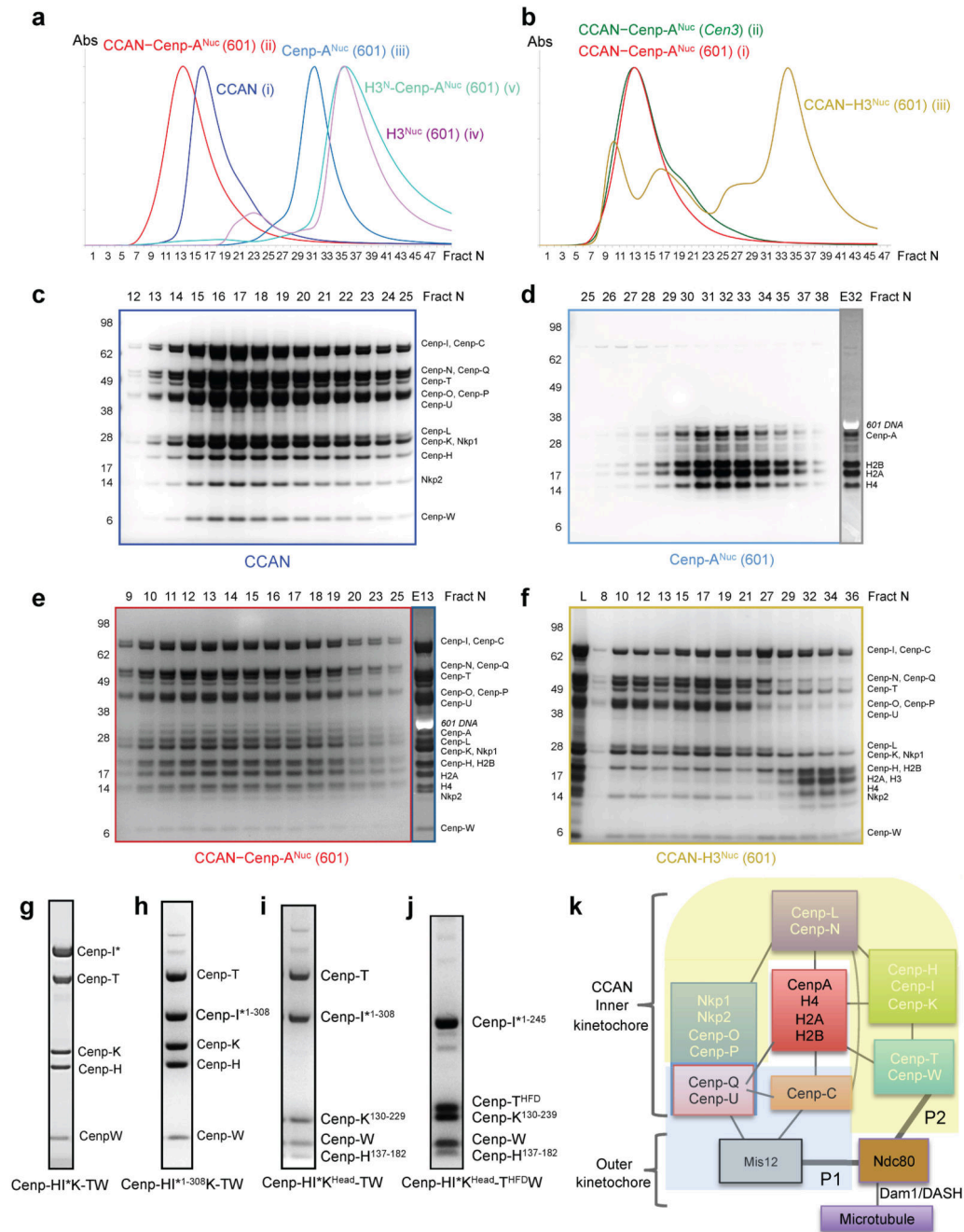
(packed in-house with ReproSil-Pur C18-AQ, 3  $\mu\text{m}$ ) coupled to a 75- $\mu\text{m}$  inner diameter 50 cm analytical column (packed in-house with Poroshell 120 EC-C18, 2.7  $\mu\text{m}$ ) (Agilent Technologies). Mobile-phase solvent A consisted of 0.1% formic acid in water, and mobile-phase solvent B consisted of 0.1% formic acid in 80% acetonitrile. A 180 min gradient was used, and start and end percentage buffer B adjusted to maximize the samples separation.

MS acquisition was performed using the MS2\_MS3 strategy: the MS1 scan was recorded in Orbitrap at a resolution of 60000, the selected precursors were fragmented in MS2 with CID and the crosslinker signature peaks recorded at a resolution of 30000. The fragments displaying the mass difference specific for DSSO were further fragmented in a MS3 scan in the ion trap (IT)<sup>57</sup>. Each sample was analysed with Proteome Discoverer 2.3 (version 2.3.0.522) with the XlinkX nodes integrated<sup>57</sup> and searching against databases generated after bottom-up analysis of the samples. The crosslink output (Supplementary Tables 1 and 2) was subsequently visualized using the xVis<sup>58</sup> web tool and the crosslinks mapped onto the cryo-EM structures of CCAN and CCAN–Cenp-A using PyMOL (Molecular Graphics System, 2.0.3, Schrodinger, LLC) (Extended Data Fig. 6e-g). The cross-linking mass spectrometry raw files, the associated output and databases are deposited through the ProteomeXchange Consortium<sup>59</sup>.

**Modelling the CCAN–Cenp-A<sup>Nuc</sup>–CBF3–Cen3 complex**—To model CCAN and CBF3 simultaneously bound to the Cenp-A nucleosome, we docked the free unwrapped DNA duplex of the CCAN–Cenp-A<sup>Nuc</sup> complex onto the CBF3–Cen3 coordinates (PDB: 6GYS)<sup>60</sup>, matching the minor and major grooves of both complexes. To avoid overlap of CBF3 and CCAN, the dyad symmetry axis of the Cenp-A nucleosome is positioned seven nucleotides upstream of the midpoint of CDEII of the *Cen3* sequence.

**Modelling *H. sapiens* and *S. pombe* Cenp-LN complexes**—To generate the *H. sapiens* Cenp-LN complex we used residues 1-207 from PDB 6EQT<sup>29</sup>, and modelled residues 208-338 and Cenp-N by one-to-one threading in PHYRE2<sup>48</sup> using *S. cerevisiae* Cenp-LN as a template. *S. pombe* Cenp-LN was modelled with PHYRE2<sup>48</sup> using *S. cerevisiae* Cenp-LN as a template. The electrostatic potential of *S. cerevisiae*, *S. pombe* and *H. sapiens* Cenp-LN complexes were calculated and displayed in PyMOL (Molecular Graphics System, 2.0.3, Schrodinger, LLC).

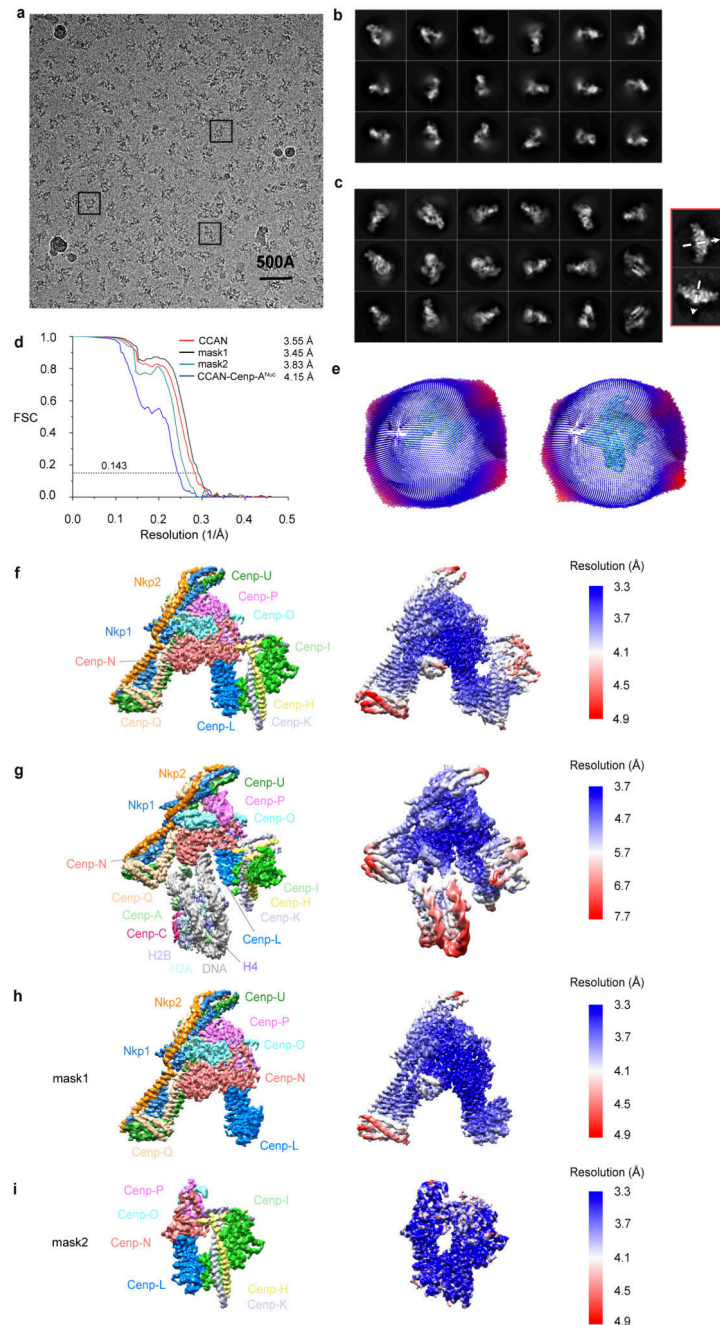
## Extended Data



### Extended Data Figure 1. Reconstituted *S. cerevisiae* CCAN-Cenp-A<sup>Nuc</sup> complexes.

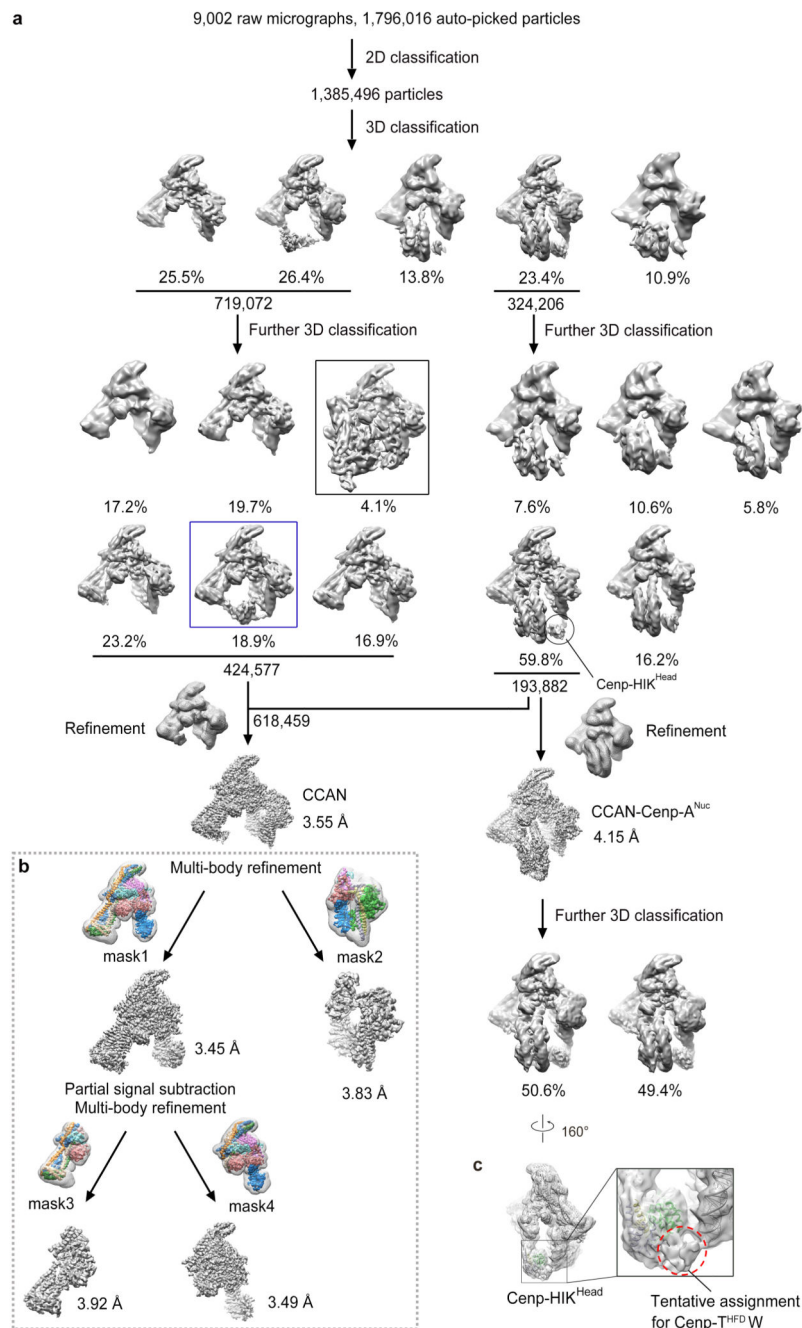
**a**, Size exclusion chromatogram profiles (Agilent Bio SEC-5 column) for (i) CCAN, (ii) CCAN-Cenp-A nucleosome (with 601) complex, (iii) Cenp-A nucleosome (with 601), (iv) H3 nucleosome (with 601) and (v) H3<sup>N</sup>-Cenp-A<sup>Nuc</sup> (with 601). **b**, Comparative size exclusion chromatogram profiles (Agilent Bio SEC-5 column) for CCAN-Cenp-A<sup>Nuc</sup> with the Cenp-A nucleosome wrapped with either the (i) 147 bp Widom 601 positioning sequence (CCAN-Cenp-A<sup>Nuc</sup> (601) – as in (a)) or (ii) a 153 bp *S. cerevisiae* centromeric *Cen3* sequence (CCAN-Cenp-A<sup>Nuc</sup> (*Cen3*)). Both complexes eluate at the same volume.

CCAN and the H3 nucleosome do not form a complex (iii). **c**, Coomassie blue-stained SDS PAGE gel of the 14 subunit CCAN complex. **d**, Coomassie blue-stained SDS PAGE gel of Cenp-A<sup>Nuc</sup> (601). Lane E32: Ethidium bromide stained gel of fraction 32. **e**, CCAN–Cenp-A<sup>Nuc</sup> (601) complex. Lane E13: Ethidium bromide stained gel of fraction 13. SEC chromatograms in **(a)**. **f**, SDS PAGE gel of CCAN and H3 nucleosome (601) SEC run shown in **(b)**. **g-j**, Coomassie blue-stained SDS PAGE gels of various Cenp-H, I and K segments co-expressed with Cenp-TW and purified with a double Strep tag on the tagged Cenp-I subunit, indicated by \*. **j**, Shows that the HFDs of Cenp-TW (Cenp-T<sup>HFDW</sup>) interacts with the Cenp-HIK<sup>Head</sup>. These results confirm the assignments of the Cenp-H, K and I subunits in our cryo-EM maps. **k**, Schematic of the organization of CCAN–Cenp-A<sup>Nuc</sup> subunits and sub-complexes and connections to the outer kinetochore Mis12 and Ndc80 complexes. Lines indicate sub-complex connections. The two pathways connecting Cenp-A<sup>Nuc</sup> to the Ndc80 complex and microtubules are indicated as P1 and P2 (thick lines to Ndc80). Subunits of the essential P1 pathway are labelled black and indicated with blue shading, whereas subunits of the non-essential P2 pathway are labelled white and indicated with yellow shading. The P2 pathway becomes essential when the P1 pathway is defective through defects in Dsn1 phosphorylation<sup>9</sup>. The experiments shown in **a-j** were performed independently in triplicate with similar results. For gel source data see Supplementary Fig. 1.



**Extended Data Figure 2. Cryo-EM data of the *S. cerevisiae* CCAN–Cenp-A<sup>Nuc</sup> complex.**  
**a**, A typical cryo-electron micrograph of CCAN–Cenp-A<sup>Nuc</sup>, representative of 9,002 micrographs. **b**, Galleries of 2D classes of CCAN, representative of 100 2D classes. **c**, Galleries of 2D classes of CCAN–Cenp-A<sup>Nuc</sup>, representative of 150 2D classes. Outlined in red are 2-D class averages for the C2-symmetric dimeric CCAN–Cenp-A<sup>Nuc</sup> complex viewed in the plane of the C2-symmetry axis. Only a few views were observed, precluding a 3D reconstruction. Cryo-EM grids partially destabilize CCAN – Cenp-A<sup>Nuc</sup> interactions, resulting in a very low abundance of dimeric CCAN–Cenp-A<sup>Nuc</sup> particles (~0.03% of total).

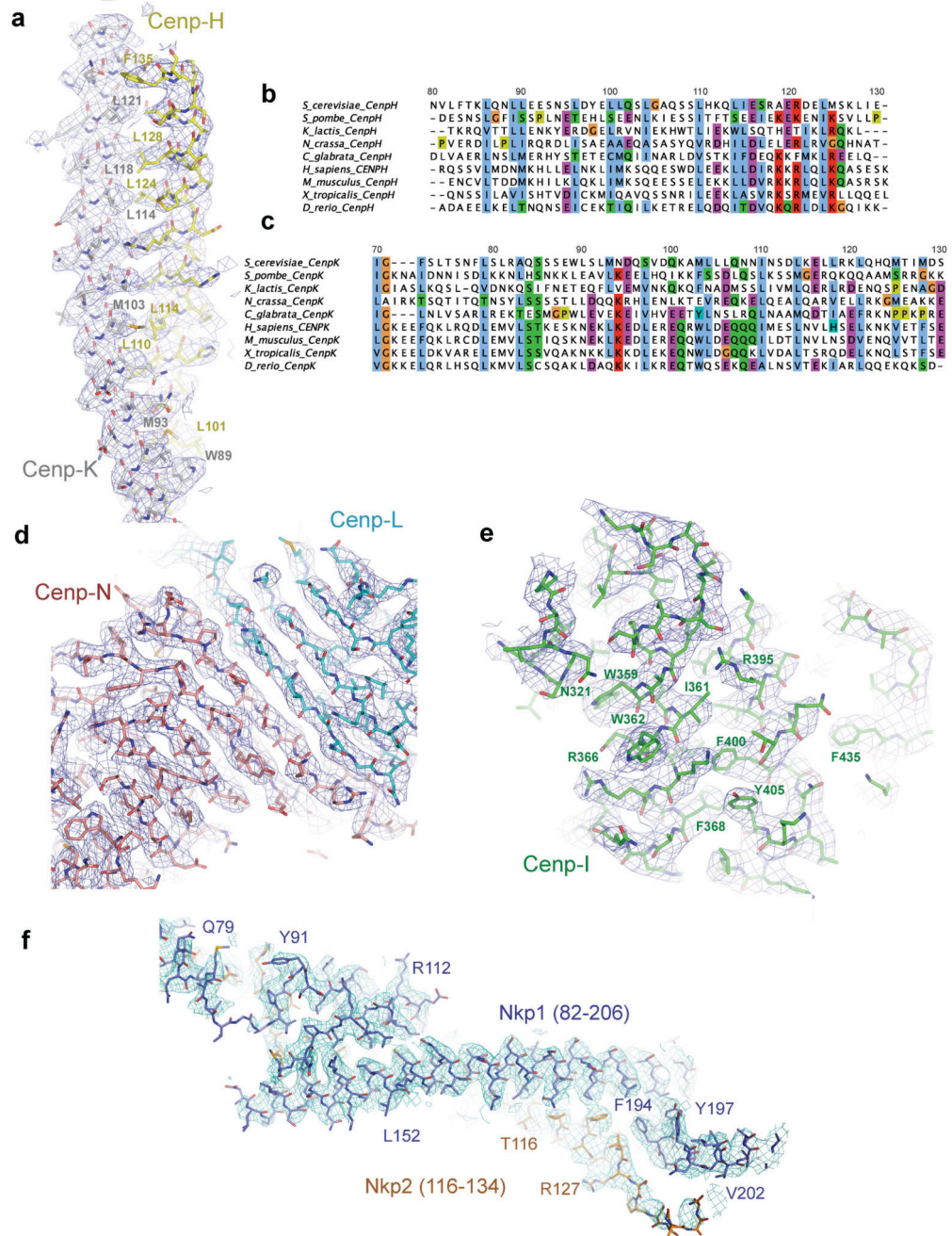
The two-fold symmetry axes of the dimeric CCAN-Cenp-A<sup>Nuc</sup> complex are shown as dashed arrows. Experiments for data in **b** and **c** were performed independently twelve times with similar results. **d**, Fourier shell correlation (FSC) curves shown for the cryo-EM reconstructions of CCAN-Cenp-A<sup>Nuc</sup> complexes: apo CCAN, mask1 (Cenp-OPQU+, Cenp-LN), mask2 (Cenp-HIK, Cenp-LN, sub-Cenp-OP), CCAN-Cenp-A<sup>Nuc</sup>. Mask1 and mask2 used for multi-body refinement are defined in **(h)** and **(i)** in and Methods. **e**, Angular distribution plot of CCAN-Cenp-A<sup>Nuc</sup> particles. **f**, Local resolution map of CCAN. **g**, Local resolution map of CCAN-Cenp-A<sup>Nuc</sup>. **h**, Local resolution map of mask1 (Cenp-OPQU+, Cenp-LN). **i**, Local resolution map of mask2 (Cenp-HIK, Cenp-LN, sub-Cenp-OP).



**Extended Data Figure 3. Workflow of 3D classification of the CCAN-Cenp-A<sup>Nuc</sup> cryo-EM data set.**

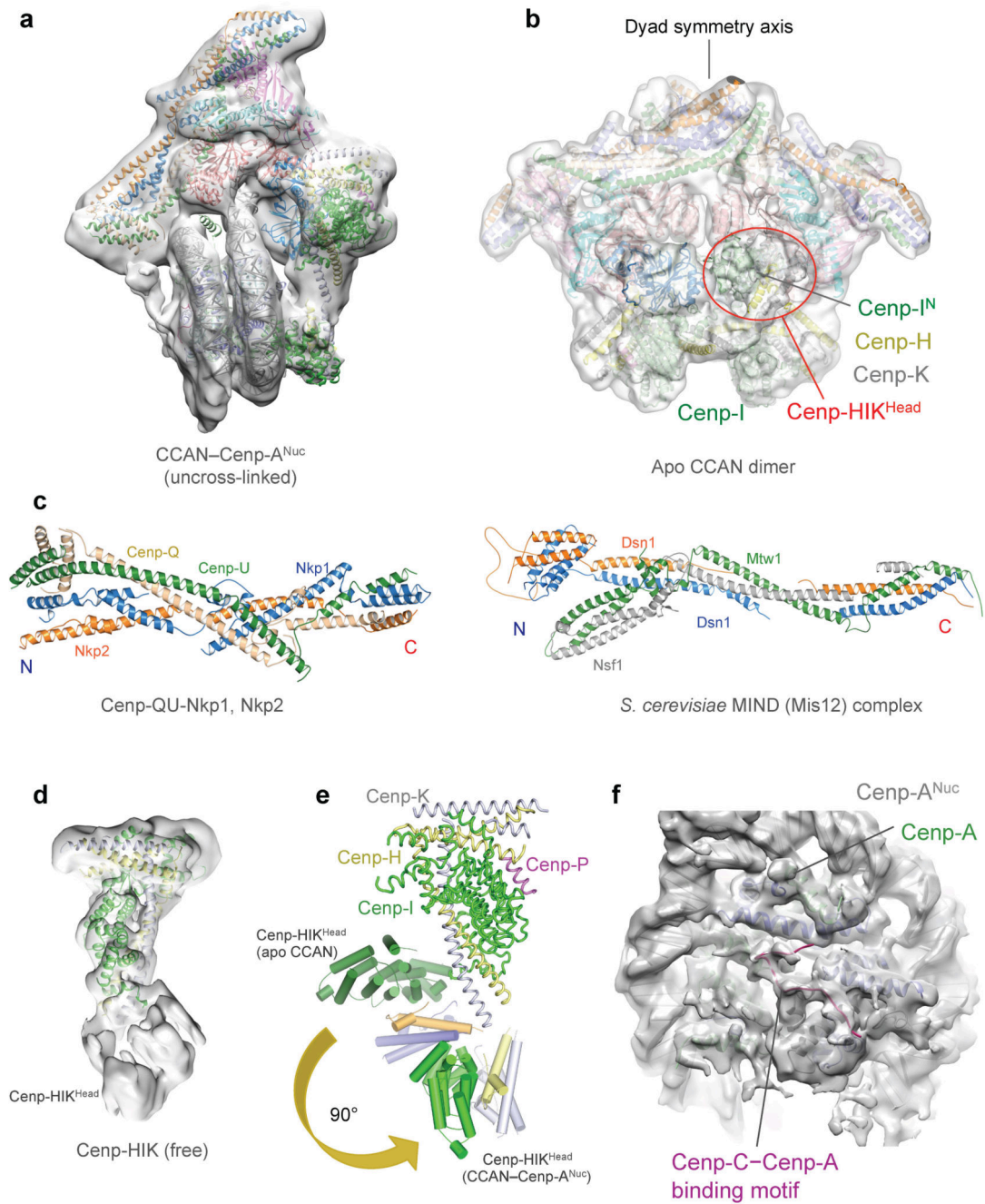
**a**, After initial 2D classification ~1.4 million particles were sorted by 3D classification into apo CCAN (52%) and the CCAN-Cenp-A<sup>Nuc</sup> complex (48%). For apo CCAN, 4% existed as dimers (black box) and 19% showed an ordered head-group (Cenp-HIK<sup>Head</sup>) for the Cenp-HIK-TW sub-complex (blue box). A mask was applied to the CCAN-Cenp-A<sup>Nuc</sup> EM map to exclude the structurally variable Cenp-HIK<sup>Head</sup> domain for reconstruction of the 4.15 Å structure. **b**, Details of the four masks used for multi-body refinement. **c**, A small 3D class

of CCAN-Cenp-A<sup>Nuc</sup> revealing density attached to Cenp-HIK<sup>Head</sup> contacting the DNA gyre of Cenp-A<sup>Nuc</sup> was assigned as Cenp-T<sup>HFDW</sup>.



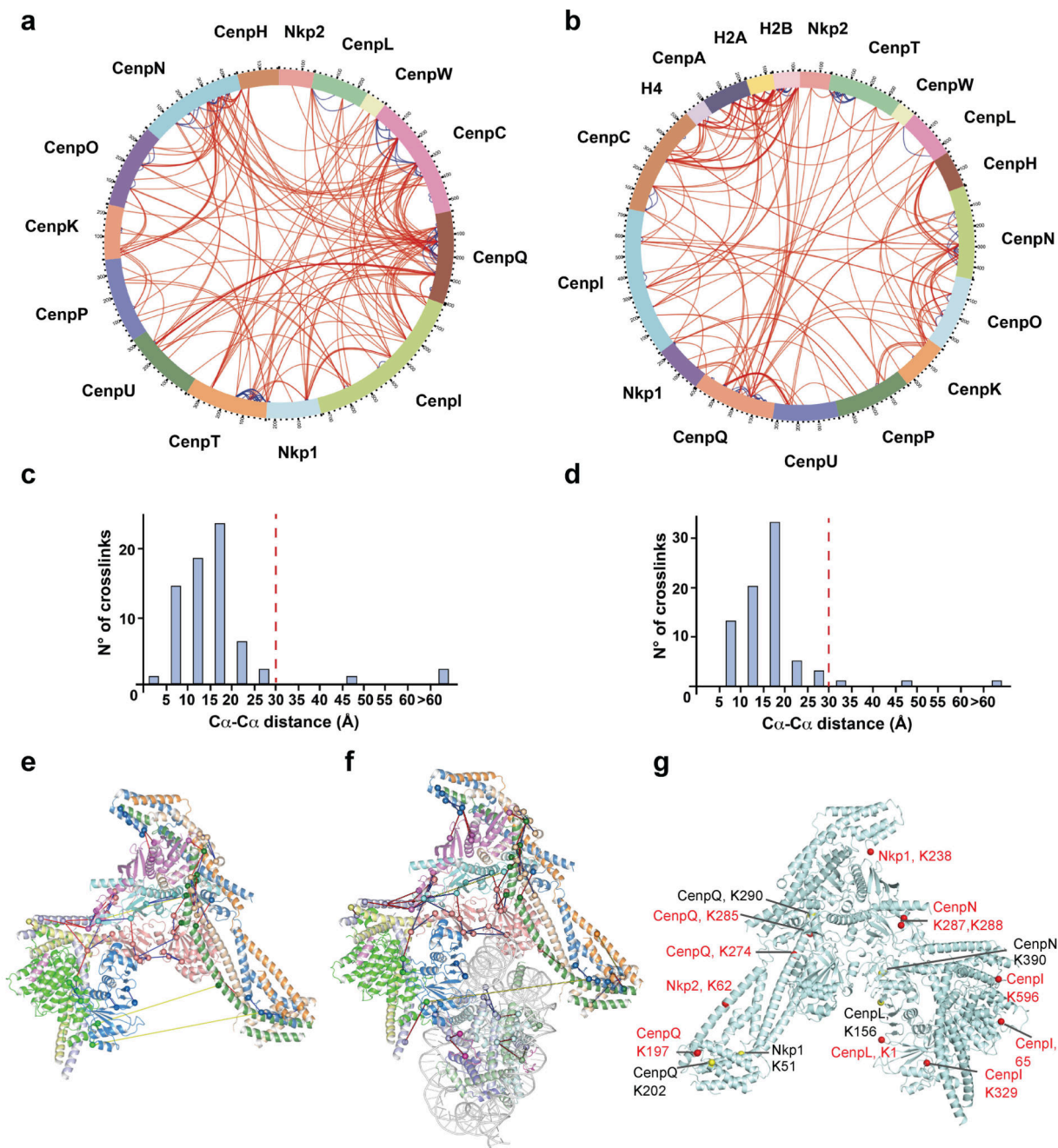
**Extended Data Figure 4. Cryo-EM density maps of apo CCAN.**

**a**, Portion of cryo-EM map for the coiled coils of Cenp-H and Cenp-K. A selection of highly conserved intersubunit residues defined in **(b, c)** are labelled. These residues are well defined in EM density, consistent with the structure. **b, c**, Multiple sequence alignment of the coiled-coil regions of **b**, Cenp-H and **c**, Cenp-K. **d-f**, Portions of cryo-EM maps for: **d**, Cenp-LN. **e**, Cenp-I. **f**, Nkp1-Nkp2. The chain assignments and polarity of Cenp-H, Cenp-I and Cenp-K of our structure agree with the cryo-EM structure of yeast Ctf3 (PDB 6OUA) 61.



**Extended Data Figure 5. Cryo-EM densities of CCAN and CCAN-Cenp-A<sup>Nuc</sup> complexes.**  
**a**, Cryo-EM reconstruction of CCAN-Cenp-A<sup>Nuc</sup> from uncross-linked sample at 8.6 Å resolution. **b**, Cryo-EM map of dimeric CCAN (also Extended Data Fig. 3a - black box). Subunits are colour-coded as in Fig. 1. The 3.5 Å monomeric free CCAN coordinates were rigid-body docked into the cryo-EM map. **c**, Cartoon representation of the *S. cerevisiae* MIND complex<sup>15</sup> (right) showing a striking similarity to the coiled coils of Cenp-QU-Nkp1-Nkp2 of CENP-OPQU+ (left). **d**, View of the 4.7 Å resolution cryo-EM map of free Cenp-HIK with fitted coordinates from CCAN. **e**, In the context of CCAN, Cenp-HIK<sup>Head</sup>

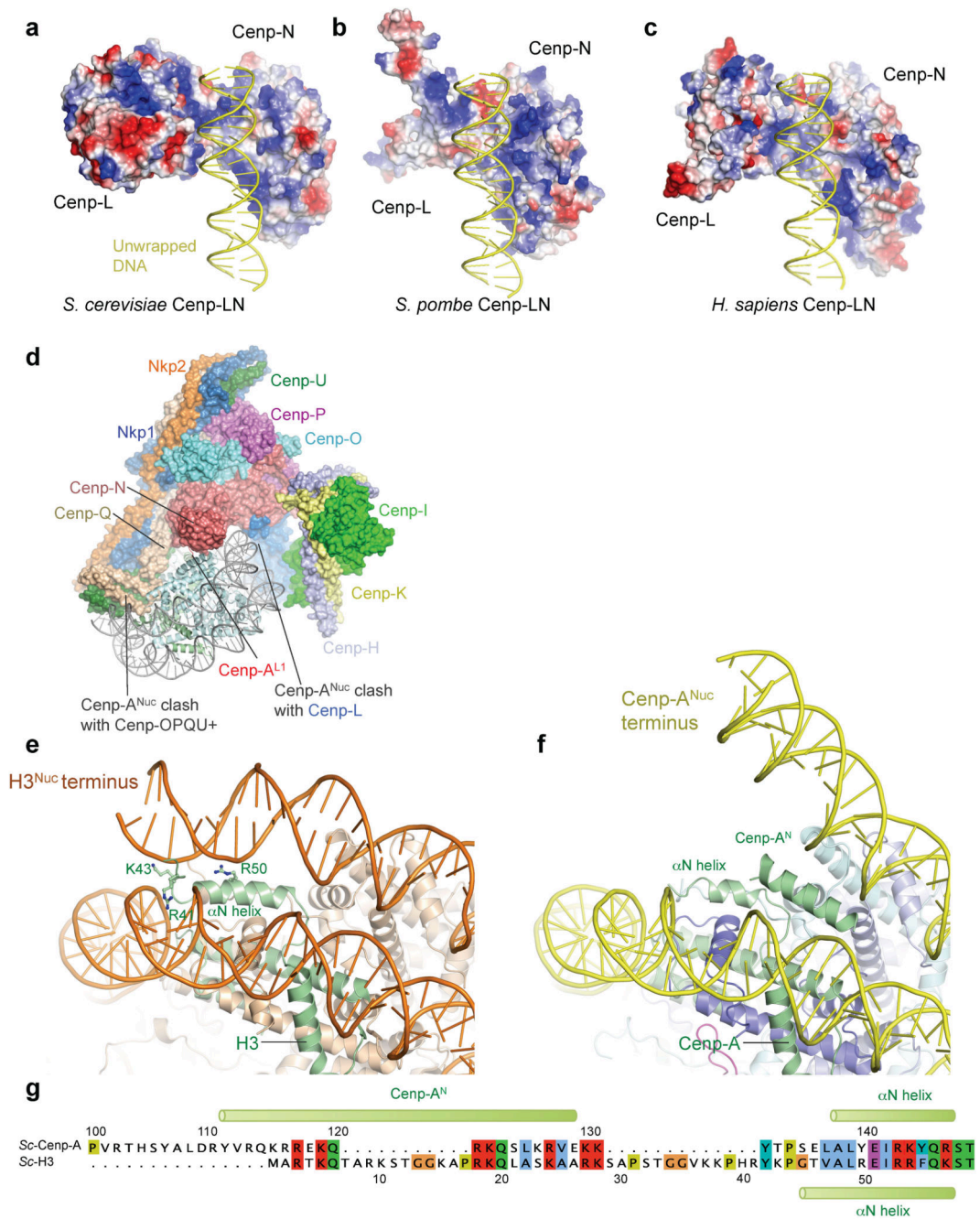
rotates to accommodate Cenp-A<sup>Nuc</sup>. The two conformations of Cenp-HIK from the apo CCAN and CCAN–Cenp-A<sup>Nuc</sup> complexes were superimposed onto their rigid portion of Cenp-HIK (C-terminal region of Cenp-I – shown for apo CCAN) to indicate the conformational variability of Cenp-HIK<sup>Head</sup> between the two states. Subunits of Cenp-HIK<sup>Head</sup> of CCAN–Cenp-A<sup>Nuc</sup> are coloured lighter. **f**, Cryo-EM density of Cenp-A<sup>Nuc</sup> showing the Cenp-C motif of Cenp-C.



**Extended Data Figure 6. Cross-linking mass spectrometry analysis of the CCAN and CCAN–Cenp-A<sup>Nuc</sup> complexes.**

**a, b**, Circular plots displaying all the identified cross-links for CCAN (**a**) and CCAN–Cenp-A<sup>Nuc</sup> (**b**). Inter- and intra-subunit cross-links are indicated in red and blue, respectively **c, d**, Histogram plots showing the Cα–Cα distance distribution of the cross-links that could be mapped onto the CCAN (**c**), and CCAN–Cenp-A<sup>Nuc</sup> structures (**d**). 95% of the mapped cross-links satisfy the cross-linker imposed distance restraint of 30 Å indicated with a dashed red line. **e, f**, Cross-links mapped onto the CCAN (**e**) and CCAN–Cenp-A<sup>Nuc</sup>

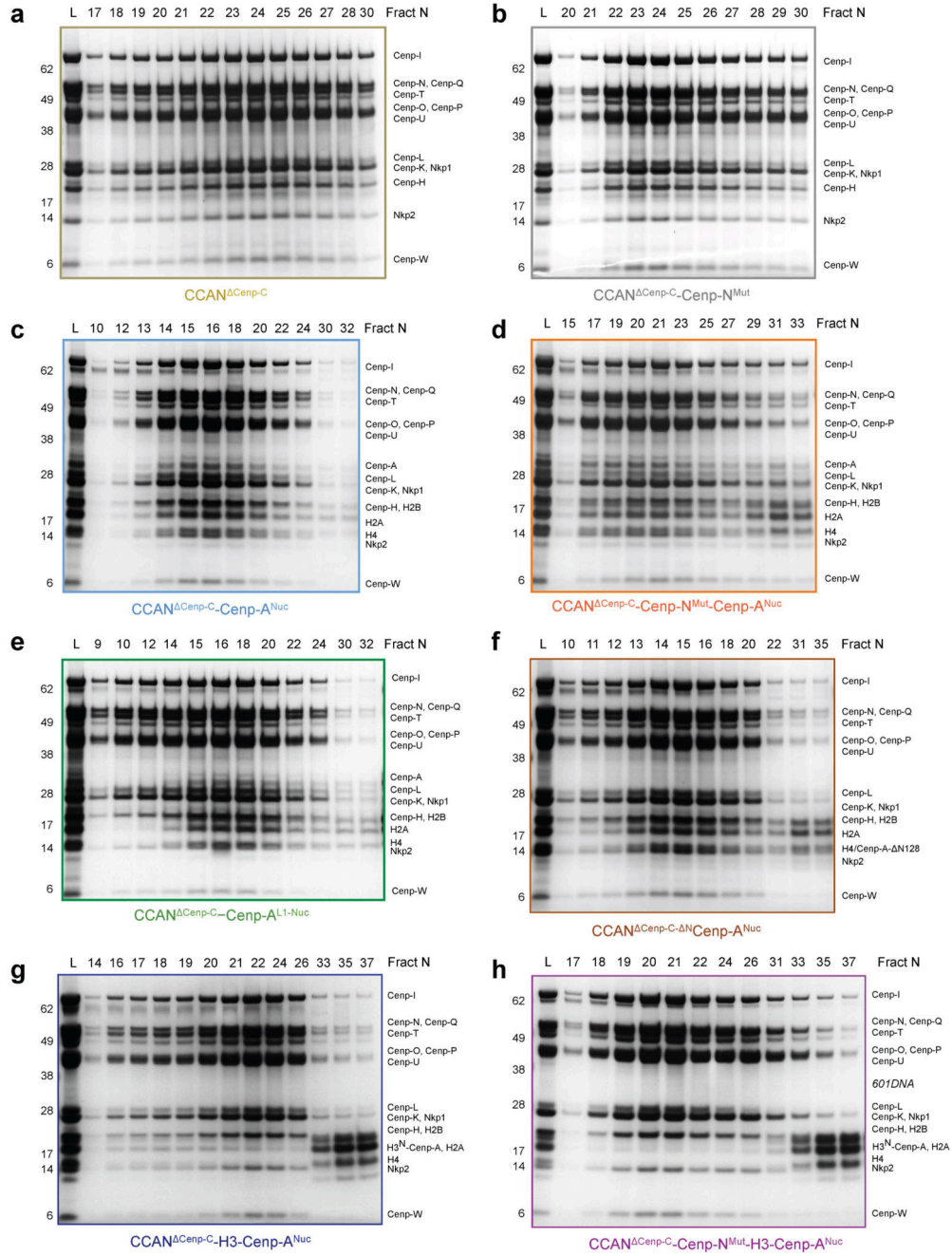
complex (**f**). Inter and intra-subunit cross-links are indicated in red and blue, respectively. Cross-links exceeding the cross-linker imposed distance restraint of 30 Å are indicated in yellow. **g**, Residues on CCAN shown by XL-MS that cross-link with Cenp-C are indicated on the CCAN structure. Red spheres: cross-links in the CCAN–Cenp-A<sup>Nuc</sup> complex. Yellow spheres: additional cross-links unique to apo CCAN. The experiments shown in **a and b** were performed independently in triplicate with similar results.



**Extended Data Figure 7. The *S. cerevisiae* Cenp-A<sup>Nuc</sup> nucleosome is unwrapped.**

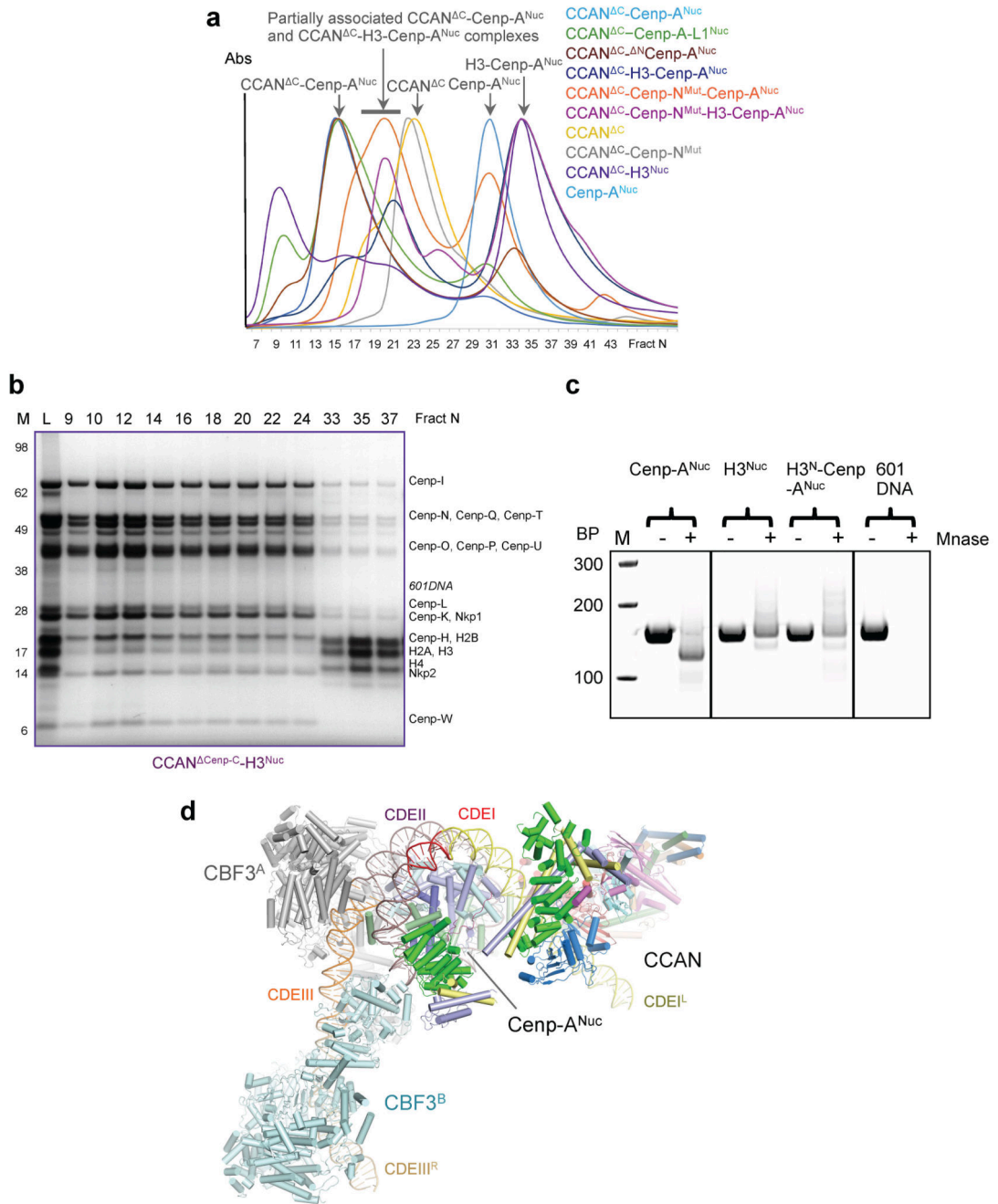
**a-c**, The positively-charged electrostatic potential of the DNA-binding groove of Cenp-LN sub-complex is conserved in *S. cerevisiae*, *S. pombe* and *H. sapiens*. *S. pombe* and *H. sapiens* are modelled structures. **d**, Cenp-N interacts with *Sc*Cenp-A<sup>Nuc</sup> in the context of CCAN differently from the interaction of free human Cenp-N with Cenp-A<sup>Nuc</sup>. The Cenp-N subunit of the human Cenp-N–Cenp-A nucleosome structure (PDB: 6C0W<sup>29</sup>) was superimposed onto Cenp-N of the *S. cerevisiae* CCAN–Cenp-A<sup>Nuc</sup> structure. In this mode of Cenp-N–Cenp-A<sup>Nuc</sup> interactions, Cenp-A<sup>Nuc</sup> would clash with Cenp-OPQU+ and Cenp-N

of CCAN. **e**, Structure  $ScH3^{Nuc}$  (PDB: 1ID3<sup>24</sup>) and **f**, Cenp-A<sup>Nuc</sup> (this work). **g**, sequence alignment of the N-terminal regions of  $ScH3$  and Cenp-A (Cse4) histones. For the chimeric  $H3^N$ -Cenp-A<sup>Nuc</sup>, residues 1-50 of  $ScH3$  were substituted for residues 1-140 of  $ScCenp-A$ . A similar approach was used for vertebrate Cenp-A<sup>Nuc</sup><sup>23</sup>.



**Extended Data Figure 8. SDS PAGE gels of CCAN <sup>Cnp-C-Cnp-A<sup>Nuc</sup></sup> complexes.**  
**a-h**, Coomassie-blue stained SDS PAGE gels of various CCAN <sup>Cnp-C-Cnp-A<sup>Nuc</sup></sup> complexes. Corresponding SEC chromatogram is shown in Fig. 4b and Extended Data Fig. 9a. **a, b**, Mutating the Cnp-N DNA binding groove did not impair CCAN <sup>Cnp-C</sup> assembly. **c**, Wild type CCAN <sup>Cnp-C</sup> forms a complex with Cnp-A<sup>Nuc</sup>. **d**, Mutating the Cnp-N DNA binding groove disrupts CCAN <sup>Cnp-C</sup> – Cnp-A<sup>Nuc</sup> interactions. **e**, Mutating the L1 loop of Cnp-A did not destabilize CCAN <sup>Cnp-C</sup> – Cnp-A<sup>Nuc</sup> interactions. **f**, Deletion of the N-terminus of Cnp-A (1-129) ( <sup>N</sup>Cnp-A<sup>Nuc</sup>) did not impair CCAN <sup>Cnp-C</sup> – Cnp-A<sup>Nuc</sup>

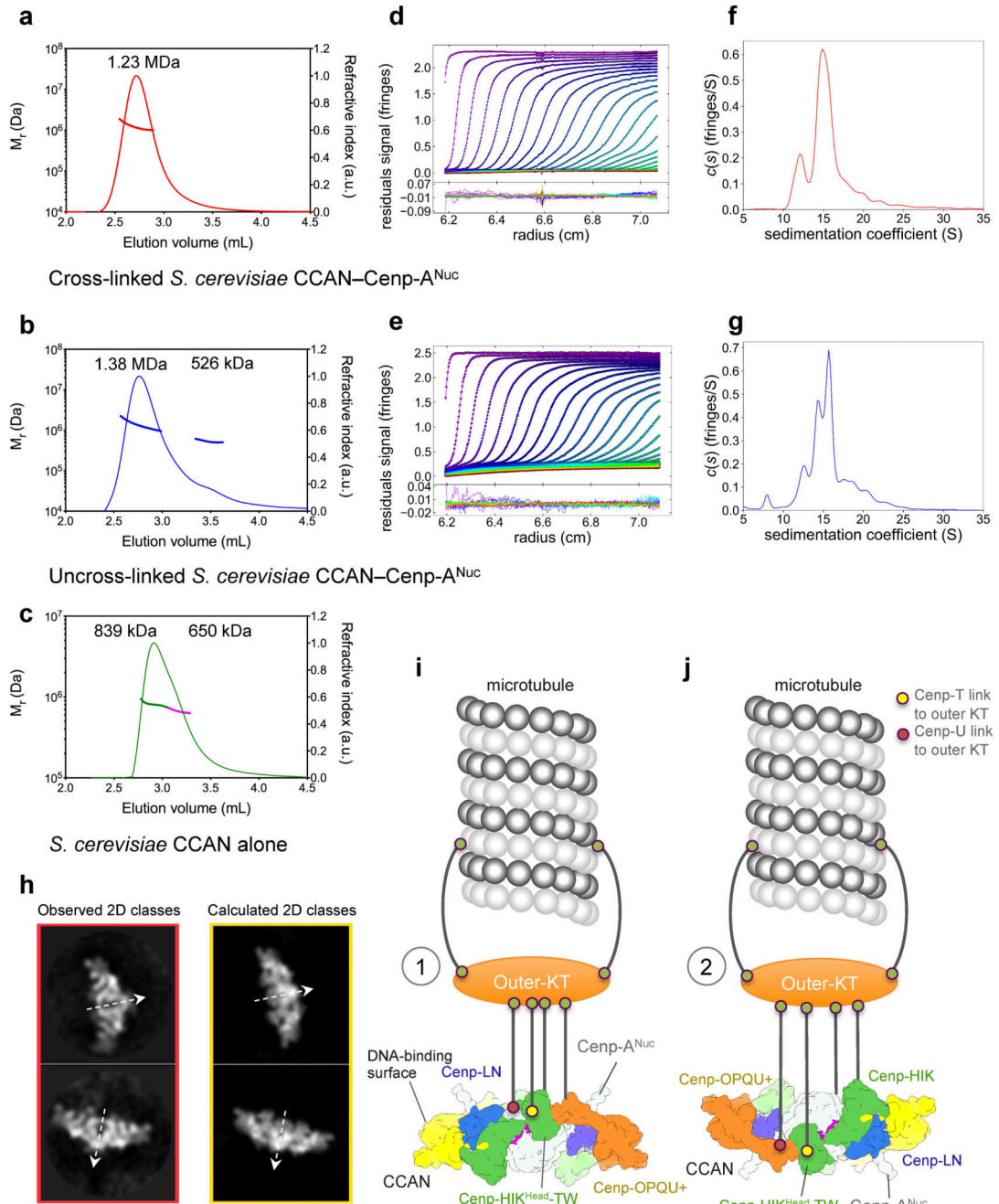
interactions. **h**, Both CCAN<sup>Cenp-C</sup> and CCAN<sup>Cenp-C-Cenp-N<sup>Mut</sup></sup> bound poorly to H3<sup>N</sup>-Cenp-A<sup>Nuc</sup>. The experiments shown were performed independently in triplicate with similar results. For gel source data see Supplementary Fig. 1.



**Extended Data Figure 9. Testing of CCAN<sup>Cnp-C</sup> binding to Cnp-A<sup>Nuc</sup>.**

**a.** Comparative size exclusion chromatogram profiles (Agilent Bio SEC-5 column) for wild type CCAN<sup>Cnp-C</sup> and the Cnp-N<sup>Mut</sup> of CCAN<sup>Cnp-C</sup> to Cnp-A<sup>Nuc</sup> and its modifications (Cnp-A<sup>Nuc</sup>-L1<sup>Nuc</sup>, <sup>N</sup>Cnp-A<sup>Nuc</sup>, H3<sup>N</sup>-Cnp-A<sup>Nuc</sup>) and H3<sup>Nuc</sup>. Mutating the L1 loop (Cnp-A-L1<sup>Nuc</sup>) of Cnp-A or deletion of the N-terminal 129 residues (<sup>N</sup>Cnp-A<sup>Nuc</sup>) did not destabilize CCAN<sup>Cnp-C</sup> – Cnp-A<sup>Nuc</sup> interactions. In contrast, CCAN with the Cnp-N<sup>Mut</sup> bound less well and both CCAN and CCAN-Cnp-N<sup>Mut</sup> bound hardly at all to H3<sup>N</sup>-Cnp-A<sup>Nuc</sup>. (CCAN<sup>C</sup> = CCAN<sup>Cnp-C</sup>). Associated SDS PAGE gels in Extended Data Fig.

8 and Extended Data Fig. 9b). **b**, Coomassie-blue stained SDS PAGE gel showed that CCAN<sup>Cenp-C</sup> did not associated with H3<sup>Nuc</sup>. **c**, Micrococcal nuclease digestion of Cenp-A<sup>Nuc</sup>, H3<sup>Nuc</sup> and H3<sup>N</sup>-Cenp-A<sup>Nuc</sup>. 601 DNA is shown as a control. The H3<sup>Nuc</sup> and H3<sup>N</sup>-Cenp-A<sup>Nuc</sup> protect a similar and longer length of DNA compared with Cenp-A<sup>Nuc</sup>. **d**, Model of CBF3<sup>60</sup> bound to CCAN-Cenp-A<sup>Nuc</sup> indicating that CBF3 would not associate with a fully assembled kinetochore, consistent with proteomic data<sup>62</sup>. The experiments shown in **a-c** were performed independently in triplicate with similar results. For gel source data see Supplementary Fig. 1.



**Extended Data Figure 10. *S. cerevisiae* CCAN-Cenp-A<sup>Nuc</sup> comprises two CCAN complexes in solution.**

The predicted mass of (CCAN)<sub>2</sub>-Cenp-A<sup>Nuc</sup> is 1.31 MDa, (CCAN)<sub>1</sub>-Cenp-A<sup>Nuc</sup> is 0.77 MDa and that for a CCAN dimer 1.09 MDa (**Extended Data Table 2**). Representative SEC-MALS data for **a**, cross-linked *S. cerevisiae* CCAN-Cenp-A<sup>Nuc</sup> complex, run independently in triplicate with similar results, average molecular mass is 1.23 MDa [(CCAN)<sub>2</sub>-Cenp-A<sup>Nuc</sup>]. **b**, uncross-linked *S. cerevisiae* CCAN-Cenp-A<sup>Nuc</sup> complex, run independently in triplicate with similar results, with average masses of 1.38 MDa [(CCAN)<sub>2</sub>-Cenp-A<sup>Nuc</sup>] and

526 kDa [(CCAN)<sub>1</sub>]. **c**, *S. cerevisiae* CCAN alone, run independently in duplicate with similar results, with average masses of 839 kDa for the leading edge (green) and 650 kDa for the trailing edge (magenta) suggesting a non-resolved monomer-dimer equilibrium. Velocity analytical ultracentrifugation of **d**, cross-linked and **e**, uncross-linked *S. cerevisiae* CCAN–Cenp-A<sup>Nuc</sup> complexes with residuals to the fits below of a c(s) distribution model: **f**, for the cross-linked complex, the major species sediments at 15.8 S ( $S_{w,20} = 26.1$  S) with a minor species at 12.1 S ( $S_{w,20} = 20.0$  S) that corresponds to calculated masses of 1.34 MDa [(CCAN)<sub>2</sub>–Cenp-A<sup>Nuc</sup>] and 896 kDa [possibly (CCAN)<sub>1</sub>–Cenp-A<sup>Nuc</sup>] respectively with a fitted value of 1.761 for the frictional ratio; **g**, for uncross-linked samples, the major species is resolved into two species that sediment at 14.3 S ( $S_{w,20} = 22.6$  S) and 15.7 S ( $S_{w,20} = 24.9$  S) with a minor species at 12.3 S ( $S_{w,20} = 19.4$  S) which gave masses of 1.32 MDa [(CCAN)<sub>2</sub>–Cenp-A<sup>Nuc</sup>] and 1.15 MDa [(CCAN)<sub>2</sub>] for the major species and 716 kDa [(CCAN)<sub>1</sub>–Cenp-A<sup>Nuc</sup>] for the minor species. The experiments shown in **d-g** were performed independently in triplicate with similar results. **h**, Examples of two 2D class averages showing the dimeric CCAN–Cenp-A<sup>Nuc</sup> particles viewed in the plane of the C2 symmetry axis (red outline) (data from Extended Data Fig. 2c) and the 2D reprojections of a modelled dimeric CCAN–Cenp-A<sup>Nuc</sup> based on the CCAN–Cenp-A<sup>Nuc</sup> cryo-EM reconstruction (yellow outline) (Extended Data Fig. 10i). There is a close correspondence in shape and dimensions between the calculated reprojections and the observed 2D classes. The two-fold symmetry axes of the dimeric CCAN–Cenp-A<sup>Nuc</sup> complex are shown as dashed arrows. **i, j**, Two alternative models for how CCAN assembled onto a Cenp-A nucleosome would interact with the outer kinetochore–microtubule interface (**Supplementary Video 2**). **i**, In scenario (1), CCAN interacts with the outer kinetochore from the same side as the DNA-binding surface. Microtubules attached to the outer kinetochore would hoist CCAN from below the over-lying nucleosome and out-stretched DNA. **j**, In scenario (2), the microtubule-outer kinetochore interface contacts CCAN from the opposite side to the CCAN-DNA binding surface. Outer-KT (outer-kinetochore): KMN network and microtubule attachment complexes: Dam1/DASH (budding yeast) and Ska proteins of vertebrates. The combined dimension of dimeric CCAN–Cenp-A<sup>Nuc</sup> (32 nm) matches that of the hub at the centre of the yeast kinetochore<sup>63</sup>.

**Extended Data Table 1**  
Cryo-EM data collection, refinement and validation statistics.

	CCAN (EMDB -4580) (PDB 6QLE)	CCAN–Cenp-A <sup>Nuc</sup> (EMDB-4579) (PDB 6QLD)	Mask1 (EMDB-4581) (PDB 6QLF)	Mask2 (EMDB-4971)
<b>Data collection and processing</b>				
Magnification	75,000	75,000	75,000	75,000
Voltage (kV)	300	300	300	300
Electron exposure (e <sup>-</sup> /Å <sup>2</sup> )	32	32	32	32
Defocus range (µm)	2.0-2.8	2.0-2.8	2.0-2.8	2.0-2.8
Pixel size (Å)	1.09	1.09	1.09	1.09

	CCAN (EMDB-4580) (PDB 6QLE)	CCAN-Cenp-A <sup>Nuc</sup> (EMDB-4579) (PDB 6QLD)	Mask1 (EMDB-4581) (PDB 6QLF)	Mask2 (EMDB-4971)
Symmetry imposed	C1	C1	C1	C1
Initial particle images (no.)	1,796,016	1,796,016	1,796,016	1,796,016
Final particle images (no.)	618,459	193,882	618,459	618,459
Map resolution (Å)	3.55	4.15	3.45	3.83
FSC threshold	0.143	0.143	0.143	0.143
Map resolution range (Å)	3.0-5.5	3.5-7.0	3.0-5.5	3.0-5.5
<b>Refinement</b>				
Initial model used (PDB code)	5MU3, 6EQT, 4JE3, 5W94	3AN2, 4X23, 5MU3, 6EQT, 4JE3, 5W94	5MU3, 6EQT, 4JE3, 5W94	5MU3, 6EQT, 4JE3, 5W94
Model resolution (Å)	3.5	4.0	3.3	-
0.143 FSC threshold				
Model resolution range (Å)	50 - 3.0	50 - 3.6	50 - 3.0	-
Map sharpening <i>B</i> factor (Å <sup>2</sup> )	-139	-108	-135	-172
Model composition				
Non-hydrogen atoms	18,058	29,183	13,541	-
Protein residues	2,401	3,172	1,790	-
Ligands	0	248	0	-
<i>B</i> factors (Å <sup>2</sup> )				
Protein	78.6	82.2	67.2	-
Ligand	-	245.8	-	-
R.m.s. deviations				
Bond lengths (Å)	0.004	0.004	0.005	-
Bond angles (°)	0.798	0.793	0.828	-
Validation				
MolProbity score	1.39	1.57	1.45	-
Clashscore	2.78	4.80	2.99	-
Poor rotamers (%)	0.11	0.08	0.19	-
Ramachandran plot				
Favored (%)	95.30	94.78	94.76	-
Allowed (%)	4.60	5.02	5.04	-
Disallowed (%)	0.10	0.20	0.20	-

## Extended Data Table 2

## Table of CCAN subunits.

Details of structured regions of CCAN subunits built into the cryo-EM density maps are indicated, including regions built as polyAla. The calculated molecular masses for CCAN and Cenp-A<sup>Nuc</sup> complexes are (i) CCAN: 543.3 kDa, (ii) CCAN dimer: 1.09 MDa, (iii) Cenp-A<sup>Nuc</sup>: 223 kDa, (iv) (CCAN)<sub>1</sub>-Cenp-A<sup>Nuc</sup>: 0.766 MDa and (v) (CCAN)<sub>2</sub>-Cenp-A<sup>Nuc</sup>: 1.31 MDa.

Subunit	<i>S.c.</i> name	Length	Mol. Mass kDa	Domain/Region 1	Domain/Region 2	Domain/Region 3	Disordered regions	Sequence built as polyA
<b>ScCenp-A nucleosome</b>								
Cenp-A	Cse4	229	26.8	α-helix and disordered 1-131	Histone fold 132-229 PDB 3AN2 <i>Hs</i> Cenp-A	-	1-111, 131-136,227-229	112-130
H2A		132	14.0	Histone fold PDB 1ID3 <i>Sc</i> H2A	-	-	-	-
H2B		132	14.2	Histone fold PDB 1ID3 <i>Sc</i> H2A	-	-	-	-
H4		103	11.4	Histone fold PDB 1ID3 <i>Sc</i> H2A	-	-	-	-
601 DNA		147 bp	90.6					
Cenp-C	Mif2	549	62.5	Cenp-C motif 283-304 PDB 4X23	Cupin fold 365-530	-	1-283,306-549	-
<b>Cenp-HIK-TW complex (ScCtf3 complex + Cenp-TW)</b>								
Cenp-H	Mcm16	181	21.1	α-helix: <i>De novo</i> 4-136	α-helix: PDB 5Z07 <i>Ct</i> Cenp-I 143-181	-	1-3,41-44,75-78,137-142	-
Cenp-I	Ctf3	733	84.3	Heat repeats PDB 5Z07 <i>Ct</i> Cenp-I 5-241	Heat repeats: <i>De novo</i>	-	242-332,526-531,597-601,620-624,657-663,677-689	321-330,664-676
Cenp-K	Mcm22	239	27.6	α-helix: <i>De novo</i> 7-128	α-helix: PDB 5Z07 <i>Ct</i> Cenp-I 143-236	-	1-6,42-49,61-68,129-142	-
Cenp-T	Cnn1	361	41.3	Histone fold		-	ND	ND
Cenp-W	Wip1	98	10.2	Histone fold		-	ND	ND

Subunit	S.c. name	Length	Mol. Mass kDa	Domain/Region 1	Domain/Region 2	Domain/Region 3	Disordered regions	Sequence built as polyA
<b>Cenp-LN complex</b>								
Cenp-L	lm13	245	28.0	$\alpha/\beta$ fold PDB 4JE3, <i>Sc</i> Cenp-L	-	-	-	-
Cenp-N	Ch14	458	52.7	Pyrim (1-102) Cenp-N fold (103-262) PDB 6EQT <i>Hs</i> Cenp-N	Cenp-N linker domain <i>de novo</i> (262-373)	Dimerization (375-468) PDB 4JE3 <i>Sc</i> Cenp-N	1-4,47-50,166-192,310-316,338-373,452-458	-
<b>Cenp-OPQU+ complex (ScCOMA+ complex)</b>								
Cenp-O	Mcm21	368	43.0	RWD PDB 5MU3 <i>K/Ctf19</i>	-	-	1-152,332-338	-
Cenp-P	Ctf19	369	42.8	RWD PDB 5MU3 <i>K/Ctf19</i>	-	-	1-96,111-123,286-292,308-313	97-110
Cenp-Q	Okp1	406	47.4	$\alpha$ -helix: <i>De novo</i>	-	-	1-160,220-228,304-319,392-406	161-219
Cenp-U	Ame1	324	37.5	$\alpha$ -helix: <i>De novo</i>	-	-	1-130,157-165,267-276	131-156
Nkp1	Nkp1	238	27.0	$\alpha$ -helix: <i>De novo</i>	-	-	1,124-135	24-32,217-238
Nkp2	Nkp2	153	17.9	$\alpha$ -helix: <i>De novo</i>	-	-	1-2,25-35	133-153

## Supplementary Material

Refer to Web version on PubMed Central for supplementary material.

## Acknowledgments

This work was funded by MRC grant (MC\_UP\_1201/6) and CR-UK grant (C576/A14109) to D.B and Horizon 2020 program INFRAIA project Epic-XS (Project 823839) to A.J.R.H. and Deutsche Forschungsgemeinschaft (EH237/12-1) to A. E.-M. We are grateful to the LMB, eBIC and the Universities of Cambridge and Leeds EM facilities for help with the EM data collection, S. Scheres for help with EM processing, members of the Barford group for useful discussions, J. Grimmett and T. Darling for computing and J. Shi for help with insect cell expression.

## References

1. Earnshaw WC, Rothfield N. Identification of a family of human centromere proteins using autoimmune sera from patients with scleroderma. *Chromosoma*. 1985; 91:313–321. [PubMed: 2579778]
2. Meluh PB, Yang P, Glowczewski L, Koshland D, Smith MM. Cse4p is a component of the core centromere of *Saccharomyces cerevisiae*. *Cell*. 1998; 94:607–613. [PubMed: 9741625]
3. Cheeseman IM. The kinetochore. *Cold Spring Harbor perspectives in biology*. 2014; 6doi: 10.1101/cshperspect.a015826
4. Musacchio A, Desai A. A Molecular View of Kinetochore Assembly and Function. *Biology*. 2017; 6doi: 10.3390/biology6010005
5. Clarke L, Carbon J. Isolation of a yeast centromere and construction of functional small circular chromosomes. *Nature*. 1980; 287:504–509. [PubMed: 6999364]
6. Winey M, et al. Three-dimensional ultrastructural analysis of the *Saccharomyces cerevisiae* mitotic spindle. *The Journal of cell biology*. 1995; 129:1601–1615. [PubMed: 7790357]
7. Furuyama S, Biggins S. Centromere identity is specified by a single centromeric nucleosome in budding yeast. *Proceedings of the National Academy of Sciences of the United States of America*. 2007; 104:14706–14711. DOI: 10.1073/pnas.0706985104 [PubMed: 17804787]
8. Camahort R, et al. Cse4 is part of an octameric nucleosome in budding yeast. *Molecular cell*. 2009; 35:794–805. DOI: 10.1016/j.molcel.2009.07.022 [PubMed: 19782029]
9. Lang J, Barber A, Biggins S. An assay for de novo kinetochore assembly reveals a key role for the CENP-T pathway in budding yeast. *eLife*. 2018; 7doi: 10.7554/eLife.37819
10. Hinshaw SM, Harrison SC. The structure of the Ctf19c/CCAN from budding yeast. *eLife*. 2019; 8doi: 10.7554/eLife.44239
11. McKinley KL, et al. The CENP-L-N Complex Forms a Critical Node in an Integrated Meshwork of Interactions at the Centromere-Kinetochore Interface. *Molecular cell*. 2015; 60:886–898. DOI: 10.1016/j.molcel.2015.10.027 [PubMed: 26698661]
12. Pesenti ME, et al. Reconstitution of a 26-Subunit Human Kinetochore Reveals Cooperative Microtubule Binding by CENP-OPQUR and NDC80. *Molecular cell*. 2018; 71:923–939 e910. DOI: 10.1016/j.molcel.2018.07.038 [PubMed: 30174292]
13. Schmitzberger F, Harrison SC. RWD domain: a recurring module in kinetochore architecture shown by a Ctf19-Mcm21 complex structure. *EMBO reports*. 2012; 13:216–222. DOI: 10.1038/embor.2012.1 [PubMed: 22322944]
14. Dimitrova YN, Jenni S, Valverde R, Khin Y, Harrison SC. Structure of the MIND Complex Defines a Regulatory Focus for Yeast Kinetochore Assembly. *Cell*. 2016; 167:1014–1027 e1012. DOI: 10.1016/j.cell.2016.10.011 [PubMed: 27881300]
15. Petrovic A, et al. Structure of the MIS12 Complex and Molecular Basis of Its Interaction with CENP-C at Human Kinetochores. *Cell*. 2016; 167:1028–1040 e1015. DOI: 10.1016/j.cell.2016.10.005 [PubMed: 27881301]

16. Hu L, et al. Structural analysis of fungal CENP-H/I/K homologs reveals a conserved assembly mechanism underlying proper chromosome alignment. *Nucleic acids research*. 2019; 47:468–479. DOI: 10.1093/nar/gky1108 [PubMed: 30407575]
17. Pekgoz Altunkaya G, et al. CCAN Assembly Configures Composite Binding Interfaces to Promote Cross-Linking of Ndc80 Complexes at the Kinetochores. *Current biology : CB*. 2016; 26:2370–2378. DOI: 10.1016/j.cub.2016.07.005 [PubMed: 27524485]
18. Guse A, Carroll CW, Moree B, Fuller CJ, Straight AF. In vitro centromere and kinetochores assembly on defined chromatin templates. *Nature*. 2011; 477:354–358. DOI: 10.1038/nature10379 [PubMed: 21874020]
19. Carroll CW, Silva MC, Godek KM, Jansen LE, Straight AF. Centromere assembly requires the direct recognition of CENP-A nucleosomes by CENP-N. *Nature cell biology*. 2009; 11:896–902. DOI: 10.1038/ncb1899 [PubMed: 19543270]
20. Carroll CW, Milks KJ, Straight AF. Dual recognition of CENP-A nucleosomes is required for centromere assembly. *The Journal of cell biology*. 2010; 189:1143–1155. DOI: 10.1083/jcb.201001013 [PubMed: 20566683]
21. Kingston IJ, Yung JS, Singleton MR. Biophysical characterization of the centromere-specific nucleosome from budding yeast. *The Journal of biological chemistry*. 2011; 286:4021–4026. DOI: 10.1074/jbc.M110.189340 [PubMed: 21115484]
22. Tachiwana H, et al. Crystal structure of the human centromeric nucleosome containing CENP-A. *Nature*. 2011; 476:232–235. DOI: 10.1038/nature10258 [PubMed: 21743476]
23. Roulland Y, et al. The Flexible Ends of CENP-A Nucleosome Are Required for Mitotic Fidelity. *Molecular cell*. 2016; 63:674–685. DOI: 10.1016/j.molcel.2016.06.023 [PubMed: 27499292]
24. White CL, Suto RK, Luger K. Structure of the yeast nucleosome core particle reveals fundamental changes in internucleosome interactions. *The EMBO journal*. 2001; 20:5207–5218. DOI: 10.1093/emboj/20.18.5207 [PubMed: 11566884]
25. Nishino T, et al. CENP-T-W-S-X forms a unique centromeric chromatin structure with a histone-like fold. *Cell*. 2012; 148:487–501. DOI: 10.1016/j.cell.2011.11.061 [PubMed: 22304917]
26. Hornung P, et al. A cooperative mechanism drives budding yeast kinetochores assembly downstream of CENP-A. *The Journal of cell biology*. 2014; 206:509–524. DOI: 10.1083/jcb.201403081 [PubMed: 25135934]
27. Anedchenko EA, et al. The kinetochores module Okp1(CENP-Q)/Ame1(CENP-U) is a reader for N-terminal modifications on the centromeric histone Cse4(CENP-A). *The EMBO journal*. 2019; 38doi: 10.15252/emboj.201898991
28. Chittori S, et al. Structural mechanisms of centromeric nucleosome recognition by the kinetochores protein CENP-N. *Science*. 2018; 359:339–343. DOI: 10.1126/science.aar2781 [PubMed: 29269420]
29. Pentakota S, et al. Decoding the centromeric nucleosome through CENP-N. *eLife*. 2017; 6doi: 10.7554/eLife.33442
30. Kato H, et al. A conserved mechanism for centromeric nucleosome recognition by centromeres protein CENP-C. *Science*. 2013; 340:1110–1113. DOI: 10.1126/science.1235532 [PubMed: 23723239]
31. Kouprina N, et al. Identification and cloning of the CHL4 gene controlling chromosome segregation in yeast. *Genetics*. 1993; 135:327–341. [PubMed: 8243998]
32. Weir JR, et al. Insights from biochemical reconstitution into the architecture of human kinetochores. *Nature*. 2016; 537:249–253. DOI: 10.1038/nature19333 [PubMed: 27580032]
33. Falk SJ, et al. Chromosomes. CENP-C reshapes and stabilizes CENP-A nucleosomes at the centromere. *Science*. 2015; 348:699–703. DOI: 10.1126/science.1259308 [PubMed: 25954010]
34. Zhang Z, Yang J, Barford D. Recombinant expression and reconstitution of multiprotein complexes by the USER cloning method in the insect cell-baculovirus expression system. *Methods*. 2016; 95:13–25. DOI: 10.1016/j.ymeth.2015.10.003 [PubMed: 26454197]
35. Schuck P. On the analysis of protein self-association by sedimentation velocity analytical ultracentrifugation. *Analytical biochemistry*. 2003; 320:104–124. [PubMed: 12895474]

36. Brautigam CA. Calculations and Publication-Quality Illustrations for Analytical Ultracentrifugation Data. *Methods in enzymology*. 2015; 562:109–133. DOI: 10.1016/bs.mie.2015.05.001 [PubMed: 26412649]
37. Samel A, Cuomo A, Bonaldi T, Ehrenhofer-Murray AE. Methylation of CenH3 arginine 37 regulates kinetochore integrity and chromosome segregation. *Proceedings of the National Academy of Sciences of the United States of America*. 2012; 109:9029–9034. DOI: 10.1073/pnas.1120968109 [PubMed: 22615363]
38. Zheng SQ, et al. MotionCor2: anisotropic correction of beam-induced motion for improved cryo-electron microscopy. *Nat Methods*. 2017; 14:331–332. DOI: 10.1038/nmeth.4193 [PubMed: 28250466]
39. Zhang K. Gctf: Real-time CTF determination and correction. *J Struct Biol*. 2016; 193:1–12. DOI: 10.1016/j.jsb.2015.11.003 [PubMed: 26592709]
40. Fernandez-Leiro R, Scheres SHW. A pipeline approach to single-particle processing in RELION. *Acta crystallographica Section D, Structural biology*. 2017; 73:496–502. DOI: 10.1107/S2059798316019276 [PubMed: 28580911]
41. Nakane T, Kimanius D, Lindahl E, Scheres SH. Characterisation of molecular motions in cryo-EM single-particle data by multi-body refinement in RELION. *eLife*. 2018; 7doi: 10.7554/eLife.36861
42. Elmlund H, Elmlund D, Bengio S. PRIME: probabilistic initial 3D model generation for single-particle cryo-electron microscopy. *Structure*. 2013; 21:1299–1306. DOI: 10.1016/j.str.2013.07.002 [PubMed: 23931142]
43. Chen S, et al. High-resolution noise substitution to measure overfitting and validate resolution in 3D structure determination by single particle electron cryomicroscopy. *Ultramicroscopy*. 2013; 135:24–35. DOI: 10.1016/j.ultramicro.2013.06.004 [PubMed: 23872039]
44. Emsley P, Lohkamp B, Scott WG, Cowtan K. Features and development of Coot. *Acta crystallographica Section D, Biological crystallography*. 2010; 66:486–501. DOI: 10.1107/S0907444910007493 [PubMed: 20383002]
45. Yang Z, et al. UCSF Chimera, MODELLER, and IMP: an integrated modeling system. *J Struct Biol*. 2012; 179:269–278. DOI: 10.1016/j.jsb.2011.09.006 [PubMed: 21963794]
46. Schmitzberger F, et al. Molecular basis for inner kinetochore configuration through RWD domain-peptide interactions. *The EMBO journal*. 2017; 36:3458–3482. DOI: 10.15252/embj.201796636 [PubMed: 29046335]
47. Hinshaw SM, Harrison SC. An Iml3-Chl4 heterodimer links the core centromere to factors required for accurate chromosome segregation. *Cell reports*. 2013; 5:29–36. DOI: 10.1016/j.celrep.2013.08.036 [PubMed: 24075991]
48. Kelley LA, Mezulis S, Yates CM, Wass MN, Sternberg MJ. The Phyre2 web portal for protein modeling, prediction and analysis. *Nature protocols*. 2015; 10:845–858. DOI: 10.1038/nprot.2015.053 [PubMed: 25950237]
49. Buchan DW, Minneci F, Nugent TC, Bryson K, Jones DT. Scalable web services for the PSIPRED Protein Analysis Workbench. *Nucleic acids research*. 2013; 41:W349–357. DOI: 10.1093/nar/gkt381 [PubMed: 23748958]
50. Luger K, Mader AW, Richmond RK, Sargent DF, Richmond TJ. Crystal structure of the nucleosome core particle at 2.8 Å resolution. *Nature*. 1997; 389:251–260. DOI: 10.1038/38444 [PubMed: 9305837]
51. Vasudevan D, Chua EY, Davey CA. Crystal structures of nucleosome core particles containing the '601' strong positioning sequence. *Journal of molecular biology*. 2010; 403:1–10. DOI: 10.1016/j.jmb.2010.08.039 [PubMed: 20800598]
52. Adams PD, et al. PHENIX: a comprehensive Python-based system for macromolecular structure solution. *Acta crystallographica Section D, Biological crystallography*. 2010; 66:213–221. DOI: 10.1107/S0907444909052925 [PubMed: 20124702]
53. Chen VB, et al. MolProbity: all-atom structure validation for macromolecular crystallography. *Acta crystallographica Section D, Biological crystallography*. 2010; 66:12–21. DOI: 10.1107/S0907444909042073 [PubMed: 20057044]

54. Goddard TD, et al. UCSF ChimeraX: Meeting modern challenges in visualization and analysis. *Protein science : a publication of the Protein Society*. 2018; 27:14–25. DOI: 10.1002/pro.3235 [PubMed: 28710774]
55. Waterhouse AM, Procter JB, Martin DM, Clamp M, Barton GJ. Jalview Version 2--a multiple sequence alignment editor and analysis workbench. *Bioinformatics*. 2009; 25:1189–1191. DOI: 10.1093/bioinformatics/btp033 [PubMed: 19151095]
56. Liu F, Heck AJ. Interrogating the architecture of protein assemblies and protein interaction networks by cross-linking mass spectrometry. *Current opinion in structural biology*. 2015; 35:100–108. DOI: 10.1016/j.sbi.2015.10.006 [PubMed: 26615471]
57. Liu F, Lossl P, Scheltema R, Viner R, Heck AJR. Optimized fragmentation schemes and data analysis strategies for proteome-wide cross-link identification. *Nature communications*. 2017; 8doi: 10.1038/ncomms15473
58. Grimm M, Zimniak T, Kahraman A, Herzog F. xVis: a web server for the schematic visualization and interpretation of crosslink-derived spatial restraints. *Nucleic acids research*. 2015; 43:W362–369. DOI: 10.1093/nar/gkv463 [PubMed: 25956653]
59. Vizcaino JA, et al. ProteomeXchange provides globally coordinated proteomics data submission and dissemination. *Nature biotechnology*. 2014; 32:223–226. DOI: 10.1038/nbt.2839
60. Yan K, Zhang Z, Yang J, McLaughlin SH, Barford D. Architecture of the CBF3-centromere complex of the budding yeast kinetochore. *Nature structural & molecular biology*. 2018; 25:1103–1110. DOI: 10.1038/s41594-018-0154-1
61. Hinshaw SM, Dates AN, Harrison SC. The structure of the yeast Ctf3 complex. *eLife*. 2019; 8doi: 10.7554/eLife.48215
62. Akiyoshi B, et al. Tension directly stabilizes reconstituted kinetochore-microtubule attachments. *Nature*. 2010; 468:576–579. DOI: 10.1038/nature09594 [PubMed: 21107429]
63. Gonen S, et al. The structure of purified kinetochores reveals multiple microtubule-attachment sites. *Nature structural & molecular biology*. 2012; 19:925–929. DOI: 10.1038/nsmb.2358

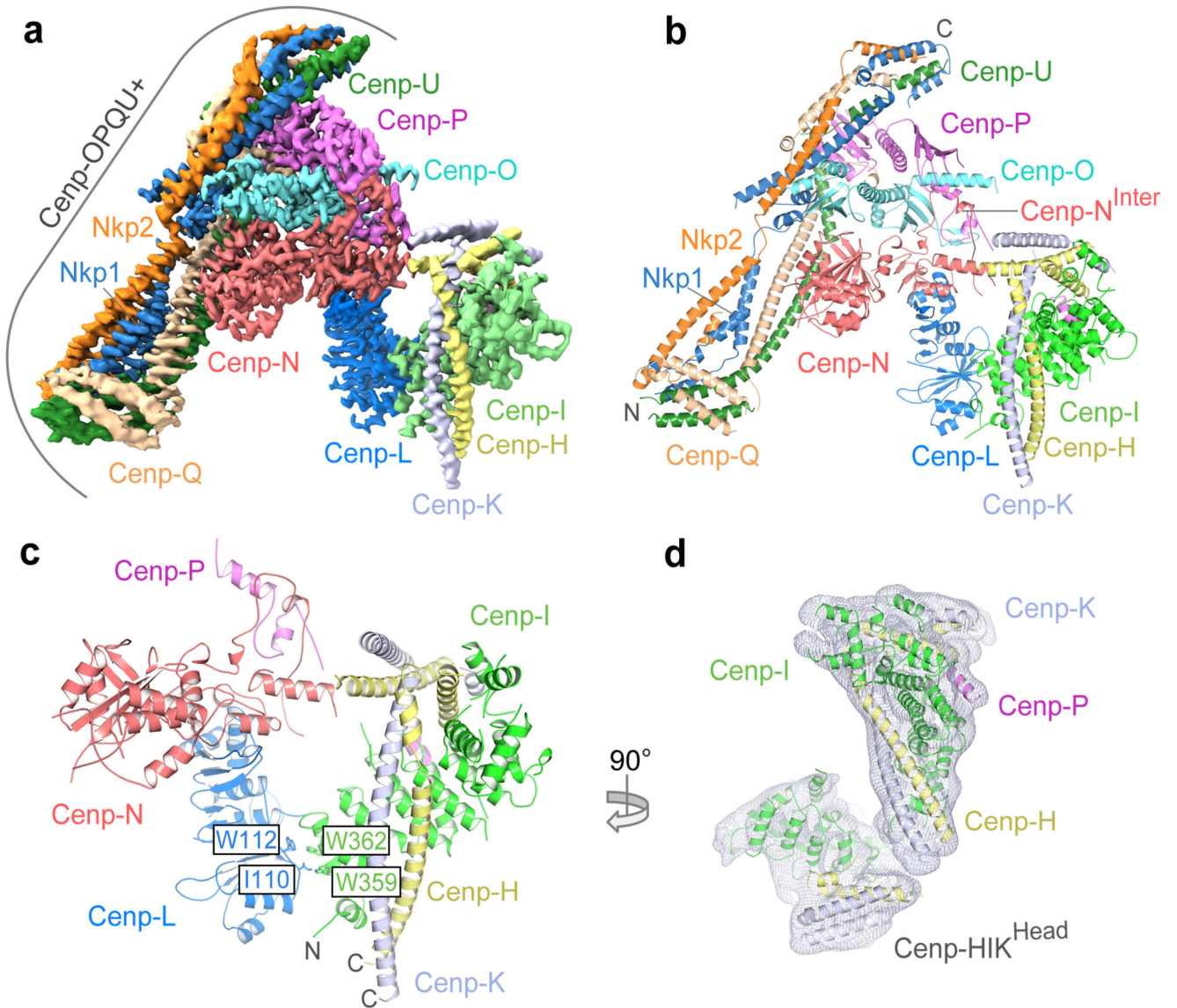


**Figure 1. Structure of the *S. cerevisiae* CCAN complex.**

**a**, Cryo-EM density map and **b**, Cartoon representation of CCAN. 11 subunits are assigned. ‘N’ and ‘C’ indicate the N- and C-termini of Cnp-QU, Nkp1 and Nkp2. **c**, Details of the Cnp-HIK–Cnp-LN modules. Residues of Cnp-I are visible from 320 onwards. **d**, Cryo-EM density for the complete Cnp-HIK module showing Cnp-HIK<sup>Head</sup> from the CCAN dimer EM 3D class (Extended Data Figs 3a and 5b).

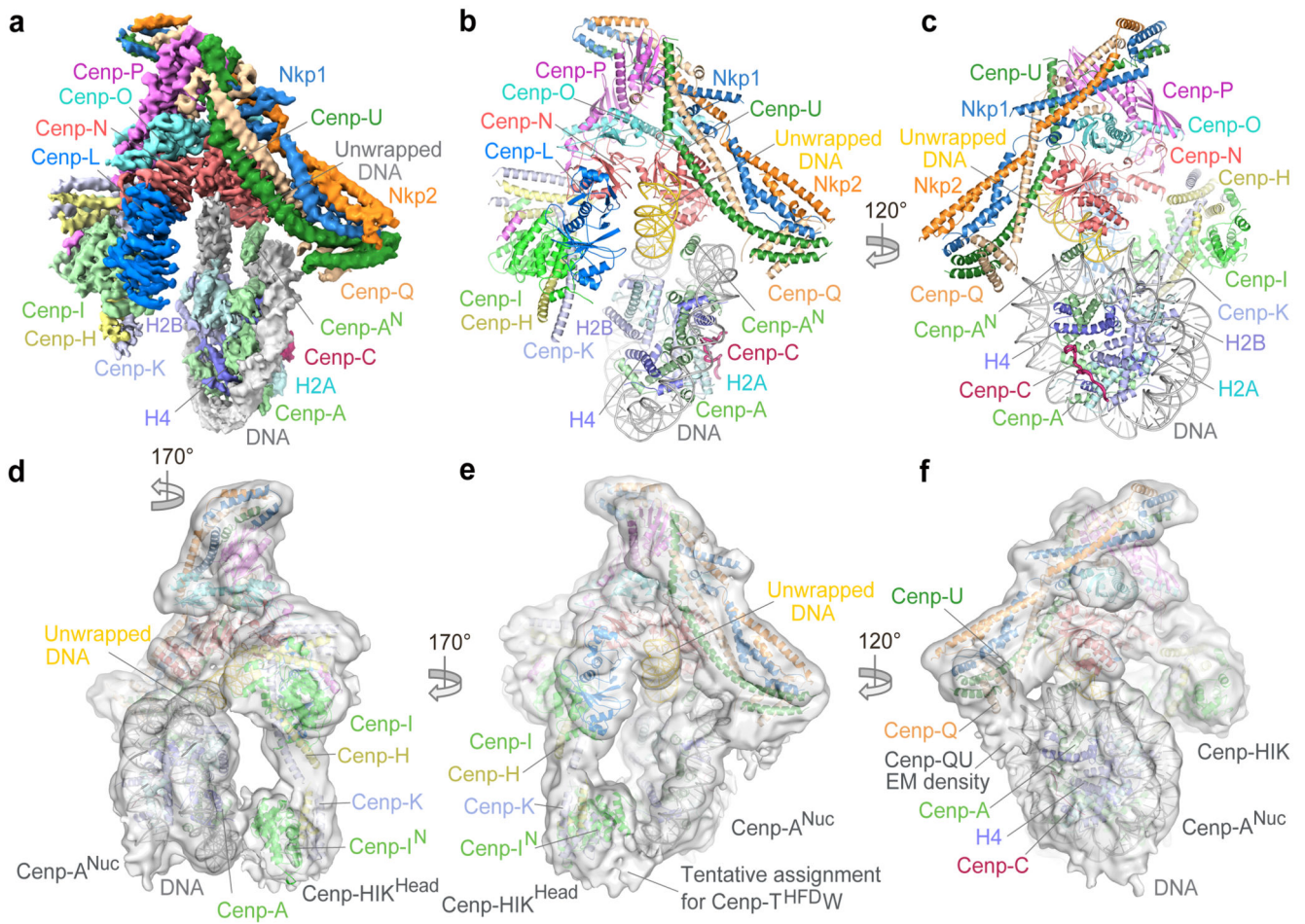


**Figure 2. Structure of the *S. cerevisiae* CCAN–Cenp-A<sup>Nuc</sup> complex.**

**a**, Cryo-EM density map of CCAN–Cenp-A<sup>Nuc</sup>. Cenp-A<sup>N</sup>: residues 111-129. **b, c**, Two views of a cartoon representation of CCAN–Cenp-A<sup>Nuc</sup>. Cenp-A<sup>Nuc</sup> wraps ~105 bp of DNA, leaving 20 bp of DNA unwrapped at both ends (coloured yellow for the ordered terminal segment). Supplementary Video 1. **d-f**, Three views of the cryo-EM density of a 3D sub-class of the overall CCAN–Cenp-A<sup>Nuc</sup> 3D class, before application of the mask used to refine the cryo-EM map shown in (a) (Extended Data Fig. 3a), highlighting contacts to Cenp-A<sup>Nuc</sup>. **d**, The Cenp-HIK<sup>Head</sup> module contacts Cenp-A. **e**, Cenp-T<sup>HFDW</sup> contacts the DNA gyre of Cenp-A<sup>Nuc</sup>. **f**, N-terminal region of Cenp-QU contacts Cenp-A and H4.

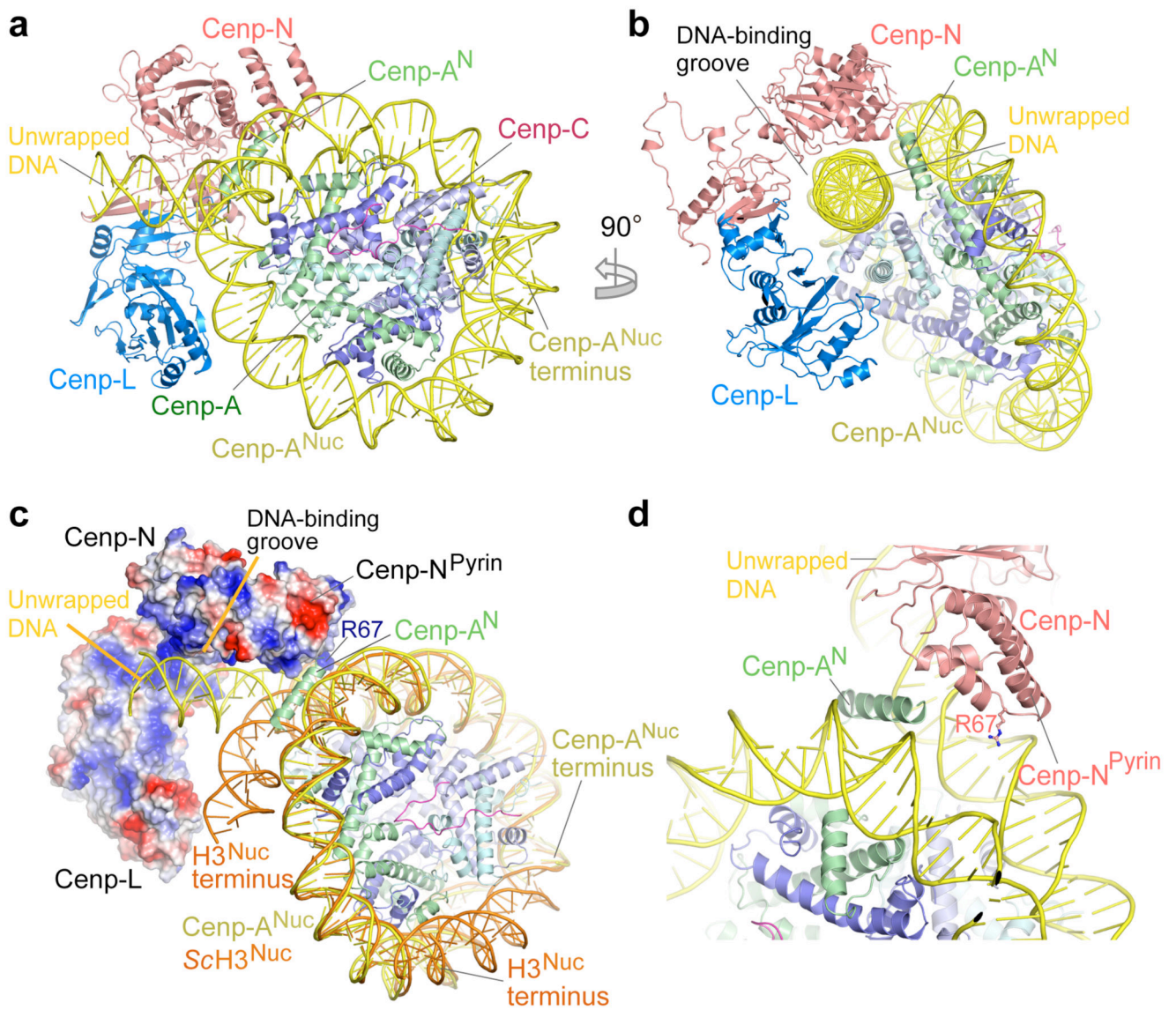


**Figure 3. CENP-LN interacts with the unwrapped DNA duplex of Cenp-A<sup>Nuc</sup>.**

**a, b.** Two orthogonal views showing the unwrapped DNA duplex of Cenp-A<sup>Nuc</sup> engaged by the DNA-binding groove of the CENP-LN sub-complex. **c.** Surface of CENP-LN showing positive electrostatic potential of the DNA-binding groove. The canonical *S. cerevisiae* H3 nucleosome (orange, PDB: 1ID3<sup>24</sup>) wraps 147 bp of DNA compared with the 105 bp wrapped by the *S. cerevisiae* Cenp-A nucleosome (yellow). **d.** Zoomed-view showing insertion of the N-terminus of Cenp-A (Cenp-A<sup>N</sup>) between the unwrapped DNA duplex and DNA gyre of Cenp-A<sup>Nuc</sup>. Arg67 of the Cenp-N Pyrin domain inserts into the DNA major groove.

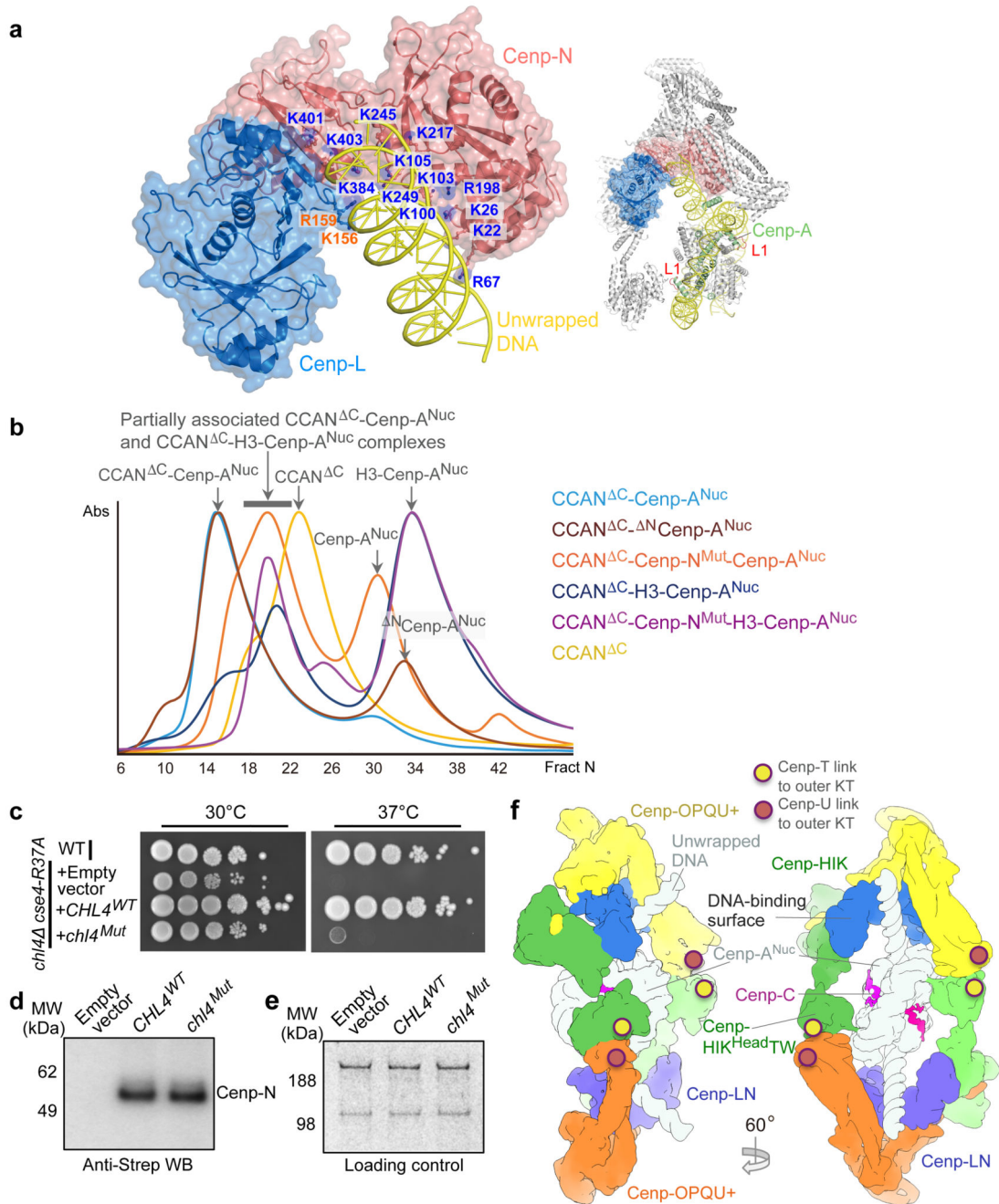


**Figure 4. The CENP-N DNA binding groove is required for stable CCAN – CENP-A<sup>Nuc</sup> interactions.**

**a**, Surface of the CENP-LN module showing the CENP-N DNA binding groove engaging the unwrapped DNA, indicating the 13 mutated Arg and Lys residues of CENP-N. Inset: overview of CCAN–CENP-A<sup>Nuc</sup> showing the CENP-A L1 loop. **b**, Size exclusion chromatograms of various CCAN<sup>CENP-C</sup>–CENP-A<sup>Nuc</sup> complexes. Wild type CCAN<sup>CENP-C</sup> forms a complex with CENP-A<sup>Nuc</sup>, but mutating the CENP-N DNA binding groove weakens CCAN – CENP-A<sup>Nuc</sup> interactions (Extended Data Fig. 8c, d). The binding of both

CCAN<sup>Cenp-C</sup> and CCAN<sup>Cenp-C-Cenp-N<sup>Mut</sup></sup> to H<sup>3</sup><sup>N</sup>-Cenp-A<sup>Nuc</sup> is severely disrupted, with little complex formed (Extended Data Fig. 8g, h). The positions of complexes are indicated by arrows. (CCAN<sup>C</sup> = CCAN<sup>Cenp-C</sup>). This experiment was performed independently in triplicate with similar results. **c**, The DNA-binding groove functions *in vivo*. Wild type Cenp-N (*CHL4<sup>WT</sup>*) rescues the growth defect of the *chl4 cse4-R73A* mutant strain at 37 °C, whereas the Cenp-N<sup>Mut</sup> (*chl4<sup>Mut</sup>*) does not. WT: wild type strain. This experiment was performed independently ten times with similar results. **d**, Western blot demonstrates that Cenp-N<sup>WT</sup> and Cenp-N<sup>Mut</sup> are expressed at equivalent levels in the *chl4 cse4-R73A* mutant strain. **e**, Loading control. Coomassie-blue stained gel shows dynein and acetyl-CoA carboxylase. Experiments in **d** and **e** were performed independently in triplicate times with similar results. **f**, Two views showing a representation of dimeric CCAN–Cenp-A<sup>Nuc</sup> complex with the second CCAN protomer generated by the dyad symmetry of Cenp-A<sup>Nuc</sup>. Sites of contact to the outer kinetochore (KT) (through Cenp-U and Cenp-T) are indicated. For gel source data see Supplementary Fig. 1.